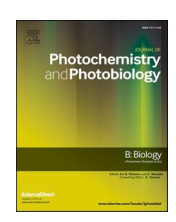
FISEVIER

Contents lists available at ScienceDirect

Journal of Photochemistry & Photobiology, B: Biology

journal homepage: www.elsevier.com/locate/jphotobiol





Attritional evaluation of lipophilic and hydrophilic metallated phthalocyanines for oncological photodynamic therapy

Lionel Mendes Dias ^{a,b,c}, Farangis Sharifi ^{c,d,1}, Mark J. de Keijzer ^{a,e,1}, Barbara Mesquita ^e, Emilie Desclos ^{c,d}, Jakub A. Kochan ^{c,d}, Daniel J. de Klerk ^a, Daniël Ernst ^a, Lianne R. de Haan ^a, Leonardo P. Franchi ^{f,8}, Albert C. van Wijk ^c, Enzo M. Scutigliani ^{c,d}, José E.B. Cavaco ^b, Antonio C. Tedesco ^g, Xuan Huang ^a, Weiwei Pan ^h, Baoyue Ding ^{a,2}, Przemek M. Krawczyk ^{c,d,2}, Michal Heger ^{a,e,*,2}, on behalf of the Photodynamic Therapy Study Group

- ^a Department of Pharmaceutics, Jiaxing Key Laboratory for Photonanomedicine and Experimental Therapeutics, College of Medicine, Jiaxing University, Jiaxing, Zhejiang, PR China
- ^b CICS-UBI, Health Sciences Research Centre, University of Beira Interior, Covilha, Portugal
- ^c Department of Medical Biology, Cancer Center Amsterdam, Amsterdam UMC, Amsterdam, The Netherlands
- d Laboratory of Experimental Oncology and Radiobiology (LEXOR), Cancer Center Amsterdam, Academic Medical Center, Amsterdam, The Netherlands
- $^{
 m e}$ Department of Pharmaceutics, Utrecht Institute for Pharmaceutical Sciences, Utrecht University, Utrecht, The Netherlands
- f Departamento de Bioquímica e Biologia Molecular, Instituto de Ciências Biológicas (ICB) 2, Campus Samambaia, Universidade Federal de Goiás (UFG), Goiânia, GO, Brazil
- g Department of Chemistry, Center of Nanotechnology and Tissue Engineering Photobiology and Photomedicine Research Group, Faculty of Philosophy, Sciences, and Letters of Ribeirão Preto, University of São Paulo, São Paulo, Brazil
- h Department of Cell Biology, College of Medicine, Jiaxing University, Jiaxing, PR China

ARTICLE INFO

Keywords:
Photosensitizers, cell death
Cell survival
Phototoxicity
Dark toxicity
Zinc phthalocyanine
Aluminum phthalocyanine

ABSTRACT

Background and aim: Oncological photodynamic therapy (PDT) relies on photosensitizers (PSs) to photooxidatively destroy tumor cells. Currently approved PSs yield satisfactory results in superficial and easy-toaccess tumors but are less suited for solid cancers in internal organs such as the biliary system and the pancreas. For these malignancies, second-generation PSs such as metallated phthalocyanines are more appropriate. Presently it is not known which of the commonly employed metallated phthalocyanines, namely aluminum phthalocyanine (AIPC) and zinc phthalocyanine (ZnPC) as well as their tetrasulfonated derivatives AIPCS4 and ZnPCS4, is most cytotoxic to tumor cells. This study therefore employed an attritional approach to ascertain the best metallated phthalocyanine for oncological PDT in a head-to-head comparative analysis and standardized experimental design.

Methods: ZnPC and AlPC were encapsulated in PEGylated liposomes. Analyses were performed in cultured A431 cells as a template for tumor cells with a dysfunctional P53 tumor suppressor gene and EGFR overexpression. First, dark toxicity was assessed as a function of PS concentration using the WST-1 and sulforhodamine B assay. Second, time-dependent uptake and intracellular distribution were determined by flow cytometry and confocal microscopy, respectively, using the intrinsic fluorescence of the PSs. Third, the LC_{50} values were established for each PS at 671 nm and a radiant exposure of 15 J/cm^2 following 1-h PS exposure. Finally, the mode of cell death as a function of post-PDT time and cell cycle arrest at 24 h after PDT were analyzed.

Results: In the absence of illumination, AIPC and ZnPC were not toxic to cells up to a 1.5- μ M PS concentration and exposure for up to 72 h. Dark toxicity was noted for AIPCS4 at 5 μ M and ZnPCS4 at 2.5 μ M. Uptake of all PSs was observed as early as 1 min after PS addition to cells and increased in amplitude during a 2-h incubation period. After 60 min, the entire non-nuclear space of the cell was photosensitized, with PS accumulation in multiple subcellular structures, especially in case of AIPC and AIPCS4. PDT of cells photosensitized with ZnPC, AIPC, and

^{*} Corresponding author at: Department of Pharmaceutics, Jiaxing Key Laboratory for Photonanomedicine and Experimental Therapeutics, College of Medicine, Jiaxing University, Jiaxing, Zhejiang, PR China.

E-mail addresses: m.heger@jctres.com, m.heger@uu.nl (M. Heger).

 $^{^{1}}$ Shared first authorship.

² Shared senior authorship..

AlPCS4 yielded LC_{50} values of 0.13 μ M, 0.04 μ M, and 0.81 μ M, respectively, 24 h post-PDT (based on sulforhodamine B assay). ZnPCS4 did not induce notable phototoxicity, which was echoed in the mode of cell death and cell cycle arrest data. At 4 h post-PDT, the mode of cell death comprised mainly apoptosis for ZnPC and AlPC, the extent of which was gradually exacerbated in AlPC-photosensitized cells during 8 h. ZnPC-treated cells seemed to recover at 8 h post-PDT compared to 4 h post-PDT, which had been observed before in another cell line. AlPCS4 induced considerable necrosis in addition to apoptosis, whereby most of the cell death had already manifested at 2 h after PDT. During the course of 8 h, necrotic cell death transitioned into mainly late apoptotic cell death. Cell death signaling coincided with a reduction in cells in the G_0/G_1 phase (ZnPC, AlPC, AlPCS4) and cell cycle arrest in the S-phase (ZnPC, AlPC, AlPCS4) and G_2 phase (ZnPC and AlPC). Cell cycle arrest was most profound in cells that had been photosensitized with AlPC and subjected to PDT.

Conclusions: Liposomal AIPC is the most potent PS for oncological PDT, whereas ZnPCS4 was photodynamically inert in A431 cells. AIPC did not induce dark toxicity at PS concentrations of up to $1.5~\mu M$, i.e., >37 times the LC50 value, which is favorable in terms of clinical phototoxicity issues. AIPC photosensitized multiple intracellular loci, which was associated with extensive, irreversible cell death signaling that is expected to benefit treatment efficacy and possibly immunological long-term tumor control, granted that sufficient AIPC will reach the tumor *in vivo*. Given the differential pharmacokinetics, intracellular distribution, and cell death dynamics, liposomal AIPC may be combined with AIPCS4 in a PS cocktail to further improve PDT efficacy.

1. Introduction

Photodynamic therapy (PDT) using the photosensitizers (PSs) porfimer sodium, 5-aminolevulinic acid (ALA) and its ester derivative, and 5,10,15,20-tetrakis(3-hydroxyphenyl)chlorin (mTHPC, Temoporfin) has been clinically approved for the treatment of various types of benign and (pre-)malignant lesions [1]. Porfimer sodium is indicated for esophageal cancer, lung adenocarcinoma, and endobronchial cancer [2]. ALA and ALA-ester are employed to treat actinic keratosis, basal cell carcinoma, and squamous cell carcinoma [3]. mTHPC is used to treat advanced head and neck squamous cell carcinoma [4]. Most PSs are associated with clinical drawbacks, which mainly entail skin phototoxicity [1] due to PS accumulation and retention in the skin as a result of the PS's lipophilicity [5]. Consequently, patients are advised to remain shielded from ambient light for 4 to 12 weeks for porfimer sodium (logP \approx 8.5) and 2 to 6 weeks for mTHPC (logP \approx 7.4) [6].

For non-terminal cancer, post-therapeutic dark periods in the order of weeks are not problematic. However, experimental PDT modalities are also being developed for incurable cancer types that are associated with a median life expectancy of less than 1 year, including pancreatic cancer [7,8] and extrahepatic cholangiocarcinoma [9-12]. Clinical studies on PDT of extrahepatic cholangiocarcinoma have yielded superior results compared to palliative chemotherapy [13,14], underscoring the need for continued translational and clinical PDT research for cholangiocarcinomas. Nevertheless, post-therapeutic dark periods of several weeks are ethically objectionable for patients diagnosed with either of these malignancies. In fact, our treatment center (Amsterdam UMC) ceased PDT of extrahepatic cholangiocarcinoma on such ethical grounds. PDT modalities for highly lethal malignancies should therefore be optimized to safely reduce the post-therapeutic dark period while preserving PDT efficacy and allow patients to have a more dignified end stage of their life.

Several research groups, including ours, have resorted to targeted photonanomedicines using liposomal encapsulation for intratumoral delivery of PSs [6]. The fundamental premise for packaging PSs into sterically stabilized liposomes is to increase the size of the pharmacological entity, such that PS passage through endothelial fenestrations in the cutaneous microcirculation is limited and dermal accumulation deterred. Endothelial fenestrations in the cutaneous microcirculation are approximately 15 nm [15,16], while lipophilic PS-encapsulating liposomes composed of dipalmitoyl phosphocholine typically have a mean diameter of 130–190 nm [9,17,18]. Secondary reasons are that liposomes can be (immuno)targeted to tumor cells [18] and tumor vascular endothelium [19], or designed to passively accumulate in the tumor stroma and disrupt the tumor microenvironment [20]. Differential targeting enables the development of liposomal PS cocktails for a more comprehensive approach to photochemical tumor destruction [6].

Moreover, concentrating the drug molecules into a liposome allows for greater pharmacodynamic action compared to the unencapsulated drug [21]. The uptake of a few liposomes loads the tumor cell with ample PS molecules to induce photokilling upon PDT. Metaphorically, this is best described by a 'Trojan Horse' (PS-loaded liposome) being transported into the cell as opposed to individual 'soldiers' (PSs) having to pass across a fortified cell wall. As a result, targeted photonanomedicines exact lower PS dosages for tumor destruction and are therefore wellsuited to ameliorate skin phototoxicity. Another strategy to reduce skin phototoxicity is to select PSs that are rapidly cleared from the circulation, yet abundantly accumulate in the tumor during their relatively short circulation time [5,22]. Hydrophilic PSs generally meet these pharmacokinetics and disposition criteria, as exemplified by the comparison between the hydrophilic PS sulfonated aluminum phthalocyanine (AlPCS) versus the fat-soluble porfimer sodium. AlPCS produced considerably less skin phototoxicity than porfimer sodium upon light exposure of photosensitized skin following equal dark periods, while also significantly outperforming porfimer sodium with respect to PDT efficacy in mouse mammary (CaD2) carcinoma [23]. A third approach to reduce skin phototoxicity is to employ PSs that have absorption bands deeper in the red spectrum [5], given the lower intensity of far-red wavelengths in sunlight (e.g., 670 nm for metallated phthalocyanines (PCs)) than shorter-red wavelengths (e.g., 630 nm for porfimer sodium) [6]. Finally, selecting PSs with high extinction coefficients lowers the dose required to induce tumor cell death [24].

Metallated PCs (Fig. 1) are PSs that structurally, photochemically, and pharmacokinetically comply with the requirements stipulated above to reduce skin phototoxicity. Metallated PCs have relatively high extinction coefficients (Fig. 1) [6] and are chemically versatile in that the octanol:water partition coefficient (logP) - and hence the degree of hydrophilicity - can be downmodulated by the conjugation of charged/ polar functional groups [23,25]. Our primary focus has been on ZnPC encapsulated into PEGylated liposomes that collectively exhibit no dark (geno)toxicity in vitro and in vivo but become toxic to tumor cells upon illumination [9,11,26,27]. Inasmuch as sulfonation of the isoindole benzo moieties of ZnPC to yield tetrasulfonated ZnPC (ZnPCS4) impairs the photoproduction of reactive oxygen species (ROS) in an aqueous environment [6], ZnPCS4 is not expected to be as toxic to tumor cells as ZnPC upon PDT. Irrespectively, some studies reported therapeutic efficacy achieved with ZnPCS4 [28-30], possibly due to the formation of oxygen-free radicals [31]. Alternatively, the lipophilic AlPC packaged into nanoparticles composed of stearic acid/oleic acid [32], stearic acid/ glyceryl behenate [33], lecithin/poloxamer 188/soybean oil/poly(D,Llactide-co-glycolide) [34], and liposomes [35,36] as well as its hydrophilic counterpart tetrasulfonated AIPC (AIPCS4) have been used for oncological PDT with encouraging outcomes in vitro and in vivo [23,37].

To date, no study has undertaken a head-to-head comparative

analysis of PDT efficacy between water-soluble liposomal ZnPC, ZnPCS4, liposomal AlPC, and AlPCS4 to ascertain the most potent PCbased PS for PDT of difficult-to-treat cancer types at minimal skin phototoxicity. In this study, we therefore encapsulated AlPC into our interstitially targeted liposomes (ITLs). The PS-ITLs have proven antitumor efficacy and safety in regard to ZnPC [9,11,26] and the formulation is known to passively accumulate in the tumor [52,53]. The ITLs further meet the low skin phototoxicity criteria by (1) being too large to extravasate through endothelial fenestrations and (2) encapsulating a PS with a Q-band absorption maximum that resides favorably in the therapeutic window and solar spectrum (i.e., greater optical penetration depth). The ZnPC-ITLs were compared to AlPC-ITLs and subsequently to their tetrasulfonated variants using an attritional approach in terms of dark toxicity, in vitro uptake and intracellular localization, and PDT efficacy, further zooming in on mode of cell death and cell cycle arrest. The main conclusion of the study is that AlPC-ITLs were the most effective PS for PDT of cultured tumor cells.

2. Materials and Methods

Supplemental material is designated with prefix 'S.' A list of abbreviations is provided in the supplemental material. The chemicals and reagents are summarized in Table S2.1. Equipment and disposables are listed in Table S2.2. Sample sizes are indicated per experiment in the results section and/or the figure legends. The concentrations listed are final unless specified otherwise. All procedures involving PSs were performed under dim light.

2.1. Materials

ZnPC and AlPC were dissolved in pyridine at a 178-μM and 150-μM stock concentration, respectively. ZnPCS4 and AlPCS4 were dissolved in

 $_{0}H_{10}N_{0}Zn$ MW: 577.900 logP: 8.50±2.62

Mutagenicity (dark): no

Tumor:healthy tissue ratio (24 h): 6.3:1 [3.7-9:1] t_{1/2}: serum ~9 h; ¹³²I-ZnPC serum ~12 h

Fluorescence: ex 647 nm, em 665 nm Q-band max: 674 nm

ε at Q-band max [M-1cm-1]: 272.000 Triplet state quantum yield: 0.57 Singlet oxygen quantum yield: 0.70

IC₅₀: NA

LC₅₀: ZnPC in cathionic liposomes: 10 μM (HUVEC); 30 μM (RAW 264.7); 25 μM (Sk-Cha1); 65 μM (A431)

LD₅₀ (dark toxicity): >5 µM (MIA)

ZnPCS4 0=\$=0 'Ζη Нό

 $C_{32}H_{16}N_8O_{12}S_4Zn$ MW: 898.190 logP: -1.7±0.4 Mutagenicity (dark): no

Tumor:healthy tissue ratio (24 h): 1.7:1

(tumor:subcutis)

t_{1/2}: NA **Fluorescence:** ex 350 nm, em 674 nm (ethanol)

Q-band max: 690 nm

ε at Q-band max [M-1cm-1]: 295.000 Triplet state quantum yield: 0.47 Singlet oxygen quantum yield: 0.43 IC₅₀: >100 µM (MCF-7, HSC-2, HCT116)

LD₅₀ (dark toxicity): >31.6 µM

AIPC

·CI

C₃₂H₁₃AICIN, **MW**: 575.0 **Mutagenicity (dark):** no MW: 575.000 logP: 8.91±2.65

Tumor:healthy tissue ratio (24 h): 16.9:1 (tumor:muscle); 5.3:1 (tumor:skin) in Cremophor

èmulsion:

 $\mathbf{t}_{1/2}$: 2.6 h (mouse plasma)

Fluorescence: ex 350 nm, em 680 nm (ethanol)

Q-band max: 680 nm

ε at Q-band max [M-1cm-1]: 126.000 Triplet state quantum yield: 0.41 Singlet oxygen quantum yield: 0.34

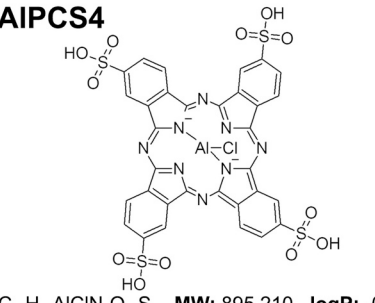
IC₅₀: NA

LC₅₀: AIPc-PVM/MA nanoparticles 0.3 µM (4T1):

0.6 µM (NIH/3T3); 1.8 µM (MCF-7);

0.5 µM (MCF-10A)

LD₅₀ (dark toxicity): >10 µM (EMT-6)



MW: 895.210 logP: -0.74±2.65

C₃₂H₁₆AICIN₈O₁₂S₄ MW: Mutagenicity (dark): no

Tumor:healthy tissue ratio (24 h): >10:1

(tumor:muscle); 2-3.5:1 (tumor:skin) $\mathbf{t}_{1/2}$: 1.5 h (plasma initial $t_{1/2}$); 70 h (minor fraction, 0.3%);

2.8 h (tumor)

Fluorescence: ex 360 nm, em 680 nm

Q-band max: 675 nm

ε at Q-band max [M-1cm-1]: 158.000 Triplet state quantum yield: 0.38 Singlet oxygen quantum yield: 0.36

IC₅₀: NA LC₅₀: NA

LD₅₀ (dark toxicity): >500 µM (T24)

Fig. 1. Molecular structure of zinc phthalocyanine (ZnPC), tetrasulfonated ZnPC (ZnPCS4), aluminum phthalocyanine (AlPC), and tetrasulfonated AlPC (AlPCS4). Photodynamic therapy-pertinent photophysical and photochemical properties as well as dark toxicity and phototoxicity are provided. Abbreviations: ε, molar extinction coefficient; em, fluorescence emission maximum; ex, excitation wavelength; IC50, half-maximal inhibitory concentration; LC50, median lethal concentration (in vitro); LD₅₀, median lethal dose (in vivo); logP, octanol:water partition coefficient; MW, molecular weight; max, maximum; t_{1/2}, circulation half-time. Values in brackets indicate range. Acronyms in parentheses refer to cell lines. Data assembled from [6,22,25,26,38-51].

phosphate-buffered saline (PBS) at a 1-mM stock concentration. All PS stock solutions were stored under a nitrogen atmosphere at room temperature (RT) (ZnPC and AlPC) or at 4 °C (ZnPCS4 and ALPCS4) in the dark. Phospholipids were dissolved in chloroform and stored under a nitrogen atmosphere at -20 °C. The phospholipid concentration of stock solutions was determined spectrophotometrically by an inorganic phosphate quantification method modified from Rouser et al. [9,54]. Physiological buffer was composed of 10 mM HEPES, 0.88% (w/v) NaCl, pH = 7.4, 0.293 osmol/kg [9].

2.2. Cell Culture

Human epidermoid carcinoma (A431) cells were cultured in T75 flasks in phenol red-containing DMEM medium supplemented with 10% fetal bovine serum (FBS), 100 U/mL penicillin, 100 µg/mL streptomycin, and 2 mM L-glutamine and grown under standard culture conditions (dark, 37 °C, humidified atmosphere composed of 5% CO $_2$ and 95% air). Cells were sub-cultured twice per week at a ratio of 1:14 to maintain a logarithmic growth phase at all stages. The cells were washed with PBS (RT, 10 mL/T75 flask) prior to detachment by incubation with Accutase (1 mL/T75 flask) for 10 min under standard culture conditions. Cells were harvested by the addition of fully supplemented DMEM and transferred to a new T75 flask.

Cells, detached as described above, were seeded into 24-well plates 24 h prior to an experiment unless stated otherwise. A seeding density of 1.5×10^5 cells/well was used to achieve $\sim\!90\%$ confluence at the time of the experiment. Cell counting was performed with an aliquot of 10 μL using a hemocytometer and a brightfield microscope.

During the experiments, DMEM without FBS and phenol red (DMEM $^{-/-}$) was used when cells were incubated with PSs or reagents.

2.3. Preparation and Characterization of ITLs

ITLs composed of DPPC and DSPE-PEG (96:4) molar ratio were prepared by the lipid film hydration technique as described previously [9]. Briefly, the phospholipids and ZnPC or AlPC were premixed at the desired ratios and the organic phase was evaporated under a stream of nitrogen gas at 40 °C in a water bath. The lipid films were vacuum exsiccated for 30 min to remove residual organic solvent and hydrated with physiological buffer. The suspension was tip sonicated and the liposomes were stored at 4 °C under a nitrogen atmosphere in the dark. The PS:phospholipid molar ratio was 0.003 [9]. The liposomes were characterized for size and polydispersity as well as zeta-potential by dynamic light scattering and electrophoretic mobility analysis, respectively, as described in [9].

2.4. Dark Toxicity

The toxicity of each PS was assessed in A431 cells in the absence of illumination. Cells seeded in 24-wells plates were washed with PBS at RT, and PS in DMEM $^{-/-}$ was added at concentrations ranging from 0 to 10 μ M for AlPCS4 and ZnPCS4, or from 0 to 1.5 μ M for AlPC-ITLs and ZnPC-ITLs (0–500 μ M phospholipid concentration). Medium containing 20% DMSO was used as positive control for complete cell death and DMEM $^{-/-}$ as negative control. After 24-, 48-, and 72-h incubation with the PS at standard culture conditions, WST-1 and SRB assays were performed as described in sections 2.8 and 2.9, respectively. Each group (PS concentration and incubation time) was measured in triplicate.

2.5. Spectral Properties of Photosensitizers

The absorption, fluorescence emission, and fluorescence excitation spectra of liposomal ZnPC and AlPC as well as ZnPCS4 and AlPCS4 were determined so that flow cytometry and confocal microscopy could be performed at the proper settings. ZnPC-ITLs and AlPC-ITLs were prepared as described in section 2.3 and diluted in physiological buffer to a

1.5- μ M PS concentration. ZnPCS4 and AlPCS4 were dissolved in physiological buffer at a 1.5- μ M concentration. For fluorescence measurements, the concentration of ZnPCS4 had to be increased to 15 μ M for optimal read-out.

Absorption was measured and corrected for physiological buffer (blank sample). Based on the absorption spectrum, the fluorescence excitation wavelength was determined: $\lambda_{ex}=650\pm5$ nm for ZnPC, ZnPCS4, and AlPC and 590 ± 5 nm for AlPCS4. Next, based on the fluorescence emission spectrum, the emission wavelength for the excitation spectrum was determined: $\lambda_{em}=707\pm5$ nm for ZnPC, ZnPCS4, and AlPC and 757 ± 5 nm for AlPCS4. Fluorescence emission and excitation spectra were read at a detector gain of 750 V and at a scan rate of 120 nm/min. Fluorescence data were corrected to 0 for the wavelength with the lowest intensity. All data were normalized to the Q band maximum. Normalized spectra were plotted in Origin software (MicroCal, Northampton, MA).

2.6. Photosensitizer-Cell Association Analysis by Flow Cytometry

The interaction between PSs and A431 cells was studied by flow cytometry. All four PS were diluted in DMEM $^{-/-}$ to a PS concentration of 375 nM, corresponding to a final phospholipid concentration of 125 μM for AlPC-ITLs and ZnPC-ITLs.

PSs were added to cells seeded in 12 wells-plates for 1-, 30-, 60-, and 120-min and incubated under standard culture conditions. After harvesting with 100 μL of Accutase for 10 min at standard culture conditions, cells were collected in 500 μL of DMEM $^{-/-}$ at RT, transferred from each well to a 2-mL centrifuge tube (Safe-lock), and centrifuged for 5 min at 500 $\times g$ and 4 °C. The supernatant was discarded, cells were resuspended in 500 μL of DMEM $^{-/-}$ at RT, and the samples were analyzed by flow cytometry.

Viable cells were gated based on their preset forward-scatter and side-scatter properties. PS autofluorescence was measured at $\lambda_{ex}=633$ nm and $\lambda_{em}=661\pm20$ nm and a fixed detector voltage (625 V). The excitation wavelength coincides with the blue Q-band absorption shoulder of the photosensitizers [6] and causes autofluorescence as a result of radiative S_1 -> S_0 state decay of a small fraction of the excited state electrons. Ten thousand events were collected in the gated region. Association was calculated from the difference between the mean fluorescence intensity of photosensitized cells relative to the mean fluorescence intensity of non-photosensitized cells (N=3 independent experiments per incubation time). Data were processed in FlowJo software (BD Biosciences, Franklin Lakes, NJ, USA).

2.7. Analysis of Photosensitizer Uptake and Intracellular Distribution by Confocal Microscopy

PS uptake and intracellular distribution were assessed by confocal laser scanning microscopy. Cells seeded in 6-wells plates containing a circular sterile 25-mm coverslip were incubated with the PS (1 mL/well) in DMEM $^{-/-}$ for 15-, 30-, and 60 min at standard culture conditions. The final PS concentrations were 10 μ M for AlPCS4 and ZnPCS4 and 3 μ M for AlPC-ITLs and ZnPC-ITLs (1 mM phospholipid concentration). Next, cells were washed with PBS (RT, 1 mL/well) prior to fixation with 2% paraformaldehyde (PFA, 1 mL/well) in PBS (RT) for 15 min in the dark. The 2% PFA in PBS was decanted, and wells were washed once with PBS at RT and immersed in 1 mL of ice-cold PBS for storage at 4 °C until confocal microscopy imaging (typically within 24 h).

Directly before imaging, 10 μ L of Hoechst 33342 (0.5 mg/mL in water) was added to each sample and incubated for 3 min at RT to stain nuclear DNA of fixed cells. Subsequently, the cover slip was secured in the steel ring of the microscope stage, 1 mL of PBS (RT) was added, and imaging was performed at the following settings: Hoechst ($\lambda_{ex}=405$ nm; $\lambda_{em}=479$ nm), ZnPC-ITLs ($\lambda_{ex}=660$ nm; $\lambda_{em}=790$ nm), AlPC-ITLs ($\lambda_{ex}=660$ nm; $\lambda_{em}=790$ nm), and AlPCS4 ($\lambda_{ex}=650$ nm; $\lambda_{em}=790$ nm). A 63 \times oil immersion objective

was used.

2.8. Mitochondrial Redox (WST-1) Assay

The WST-1 colorimetric assay was performed to determine mitochondrial redox state [55] as part of *in vitro* PS toxicovigilance. The ZnPC and AlPC have a logP of >8 and hence localize to cell and organelle membranes, including mitochondria [6]. Inasmuch as mitochondria play a key role in cell death, particularly when the electron transport chain is dysregulated [56], a mitochondrial redox function assay was selected to gauge dark toxicity of the PSs. The WST-1 assay is ideal because it does not notably interfere in cell physiology, allowing subsequent cell viability analysis by other methods.

Briefly, cells were washed once with PBS (37 °C). WST-1 reagent was added to DMEM $^{-/-}$ at a 1:25 volume ratio. A 300-µL aliquot was transferred to each well (for 24-wells plates) and cells were incubated for 20 min under standard culture conditions. After incubation, 100 µL of the medium containing WST-1 was transferred in duplicate to a 96-wells plate. The absorption was read using a plate reader at 450 nm and a reference wavelength of 620 nm for background subtraction. The background-corrected mean \pm SD absorption at 450 nm was calculated per concentration and incubation time (N=3) and normalized to the mean WST-1 absorbance of untreated cells (N = 3). Finally, the remainder of the WST-1-containing medium was removed by washing once with PBS (37 °C) using a squirt bottle and processed further for total protein content as described in the next section.

2.9. Cell Viability (SRB) Assay

The sulforhodamine B (SRB) colorimetric assay was used to measure total protein content as a more definitive parameter of cytotoxicity. This assay is based on the premise that dead and late-stage dying cells detach from the well plate bottom, leaving only viable cells that are stained and semi-quantified [57].

Following the single wash, cells were tapped dry and fixed with 300 μL of 10% ice-cold trichloroacetic acid in Milli-Q for at least 1 h at 4 °C. Next, the cells were washed $5 \times$ with Milli-Q (RT) using a squirt bottle and stained with 0.4% SRB dissolved in 1% acetic acid in Milli-Q for at least 15 min (300 $\mu L/\text{well}$ for a 24-well plate). The SRB solution was decanted, and the cells were washed 4 \times with 1% acetic acid in a squirt bottle (RT) to remove unbound SRB. The well plate was left to dry at $37~^{\circ}\text{C}$ for at least 15 min. Once dried, $500~\mu\text{L}$ of 10 mM unbuffered TRIS base in Milli-Q (RT) was added to each well and the plate was gently rocked for at least 1 min to completely dissolve the SRB. Absorption was measured in a microplate reader at 564 nm and 600 nm and a reference wavelength of 690 nm for background correction. The corrected mean \pm SD absorption at 564 nm was calculated per concentration and incubation time and normalized to the corrected mean SRB absorbance of untreated cells (N = 3/group). Absorbance data at 600 nm were used to determine cell viability when the optical density of the 564-nm read was

2.10. PDT of Cultured Cells

To compare photodynamic efficacy between the PSs, mitochondrial redox state and total protein content were measured after PDT. Cells seeded in 24-wells plates were incubated for 1 h with PS in DMEM $^{-/-}$ as described in section 2.2. Next, cells were washed once with PBS (RT, 500 $\mu L/well$) and received fresh DMEM $^{-/-}$ (37 °C, 500 $\mu L/well$). The cells were illuminated with a 671-nm solid state diode laser at 500 mW for 57 s/well (the diameter of the beam was equal to the diameter of each well; 15.6 mm), equating to a cumulative radiant exposure of 15 J/cm 2 per well. The laser output power was confirmed with a power meter before every illumination. A black surface was placed below the 24-wells plate to absorb stray light during illumination. Following illumination, the cells were incubated in DMEM $^{-/-}$ for 4 h or 24 h at standard culture

conditions to emulate PDT-induced malnutrition due to vascular shutdown [58,59]. Lastly, the WST-1 assay followed by the SRB assay were performed as described in sections 2.8 and 2.9, respectively. The results were normalized to the mean of illuminated control cells incubated in only medium (N=3/group). Graphs and LC₅₀ values were obtained using the non-linear fit data analysis in Prism (GraphPad Software, San Diego, CA, USA).

2.11. Analysis of Mode of Cell Death

Cell death was characterized according to phosphatidylserine externalization (indicative of apoptosis) and plasma membrane disruption (indicative of necrosis), which were analyzed by flow cytometry. Cells seeded in 12-well plates were treated by PDT as described in section 2.10. Illumination was performed at 500 mW for 1 min and 54 s, accounting for a cumulative radiant exposure of 15 J/cm² per well. The plate was kept at 37 °C using a plate heater during PDT. After 2 h, 4 h, and 8 h of incubation at standard culture conditions (N = 3 per time point), the medium was transferred into 15 mL sterile centrifuge tubes, along with the attached cells that were harvested following trypsinization (100 uL of Accutase for 10 min at standard culture conditions). Cells were then centrifuged at $500 \times g$ for 5 min and 4 °C. The supernatant was decanted, and the cell pellet was resuspended in 100 μ L of 1 \times annexin V binding buffer (RT) containing 5 µL of Alexa Fluor 488-conjugated annexin V. The annexin V binding buffer was diluted 5 \times with Milli-Q. After 15-min incubation at RT, 399 µL of diluted annexin V binding buffer was added, and the cell suspension was transferred to 5-mL round-bottom flow cytometry tubes. Subsequently, 1 µL of propidium iodide (PI, 0.1 mg/mL diluted annexin V binding buffer) was added 5 min prior to flow cytometry. Cells were gated based on forward scatter and sideways scatter properties. Cell remnants and cell-derived microparticles were gated out. Annexin V and PI fluorescence was measured at $\lambda_{ex} = 488$ nm, $\lambda_{em} = 530 \pm 30$ nm and $\lambda_{ex} = 488$ nm, $\lambda_{em} = 670$ nm long pass filter, respectively. Ten thousand events were collected in the gated region. The scatterplots were analyzed in FlowJo software, where quadrants were positioned based on the green and red fluorescence of untreated cells. Viable cells were quantified as annexin V-negative / PInegative, while cells that were in early apoptosis were quantified as annexin V-positive / PI-negative. Cells in late apoptosis and necrosis were clustered and quantified as annexin V-positive / PI-positive and annexin V-negative / PI-positive, respectively (modified from [60]). Data were plotted in Prism.

2.12. Cell Cycle Analysis

To determine the effects of PDT on cell cycle phases (DNA content; G₀/G₁, S, and G₂/M), PDT-treated cells were stained with PI and analyzed by flow cytometry [10,12,17]. Cells seeded in 12-well plates were incubated for 60 min with PS (ZnPC-ITLs and AlPC-ITLs, $31.25 \mu M$ PS concentration; ZnPCS4 and AlPCS4, 0.31 μM) in DMEM^{-/-} (37 °C, 1000 μ L/well). After washing with PBS (37 °C), fresh DMEM^{-/-} was added and cells were illuminated as described in section 2.11 (N = 3 per PS) or kept in the dark (control cells). Cells were harvested 24 h after PDT (or incubation in the dark) with Accutase (100 μ L/well, 10 min at standard culture conditions) in 1 mL of PBS (RT). The cells were transferred to 15-mL sterile centrifuge tubes and washed twice by centrifugation at 500 \times g for 5 min and 4 °C. Following the second centrifugation step, the supernatant was decanted and the pellet was resuspended in 300 μ L of PBS (RT). Cells were fixed by dropwise addition of 700 μ L of ice-cold 96% ethanol under continuous swirling. PBS (1 mL at RT) was added and cells were centrifuged for 5 min at 500 $\times g$ and 4 $^{\circ}C$. The supernatant was discarded and cells were resuspended in 200 μL of PI staining solution (20 $\mu g/mL$ PI and 100 $\mu g/mL$ RNAse A in PBS) in 300 μL of PBS (RT). Flow cytometry was performed as described for PI in section 2.11. The percentage of the cell population in the GO/G1 phase, S phase, and G2/M phase was calculated applying the Watson (Pragmatic)

univariate model [61] in FlowJo.

3. Results and Discussion

3.1. The Utility of Passive Tumor Targeting by Metallated Phthalocyanines as Part of a Comprehensive Tumor-Targeting Photosensitizer Platform and the Need for Systematic Photosensitizer Selection

Solid tumors in internal organs essentially have three druggable targets for PDT: the tumor cells that make up the tumor parenchyma, the intratumoral vasculature that supplies the tumor with oxygen and nutrients, and the tumor interstitial space that forms the tumor microenvironment [6]. We have developed and tested PEGylated liposomal photomedicines for each of these targets, which are dubbed tumor cell-targeting liposomes (TTLs) [18], endothelium-targeting liposomes (ETLs) [10,12,17,26,62], and ITLs [9,11], respectively. These liposomal formulations are intended to deliver PSs to the tumor (Fig. 2) and can be combined into a single cocktail for intravenous administration to comprehensively photosensitize key anatomical sites of the tumor. Multi-targeted photosensitization reduces the opportunity for PDT-subjected tumor cells to recover from photochemically-induced hyperoxidative stress [63] via the activation of survival pathways [64], as has been shown to occur following PDT [11,26].

This study is centered on interstitial targeting and the ITL component of the platform. The lipophilic PS-containing ITLs are directed into the tumor by passive diffusion through leaky intratumoral vasculature in accordance with the enhanced permeability and retention (EPR) effect [52,53]. Compositionally similar formulations have been clinically approved and are used in oncological patients to deliver chemotherapeutics such as doxorubicin [67,68], vincristine [69,70], and irinotecan [71] to tumors. The EPR-based passive targeting equally applies to water-soluble PC derivatives (ZnPCS4 and AlPCS4); an alternative to ITL-based tumor photosensitization and second focus of this study. AlPCS4 was demonstrated to abundantly accumulate in tumor xenografts 2–4 h following intravenous administration [22,25]. The pharmacokinetics of hydrophilic PC derivatives depend on the degree of sulfonation and generally follow an inverse relationship between rate of intratumoral accumulation and the logP of the PC derivative [22,72,73].

The eventual localization of the PC-based PSs that passively diffuse into tumors is currently elusive. The intratumoral sites that become photosensitized ultimately dictate the tumoricidal efficacy [6,74]. Photosensitization of tumor cells is most critical insofar as hyperoxidative stress in parenchymal cells inflicts direct damage to key components that leads to activation and execution of cell death mechanisms that in turn prime a subsequent anti-tumor immune response [75]. Photosensitization of multiple intracellular loci is preferable for therapeutic outcome [6,74,76]. Oxidative damage to cellular and non-

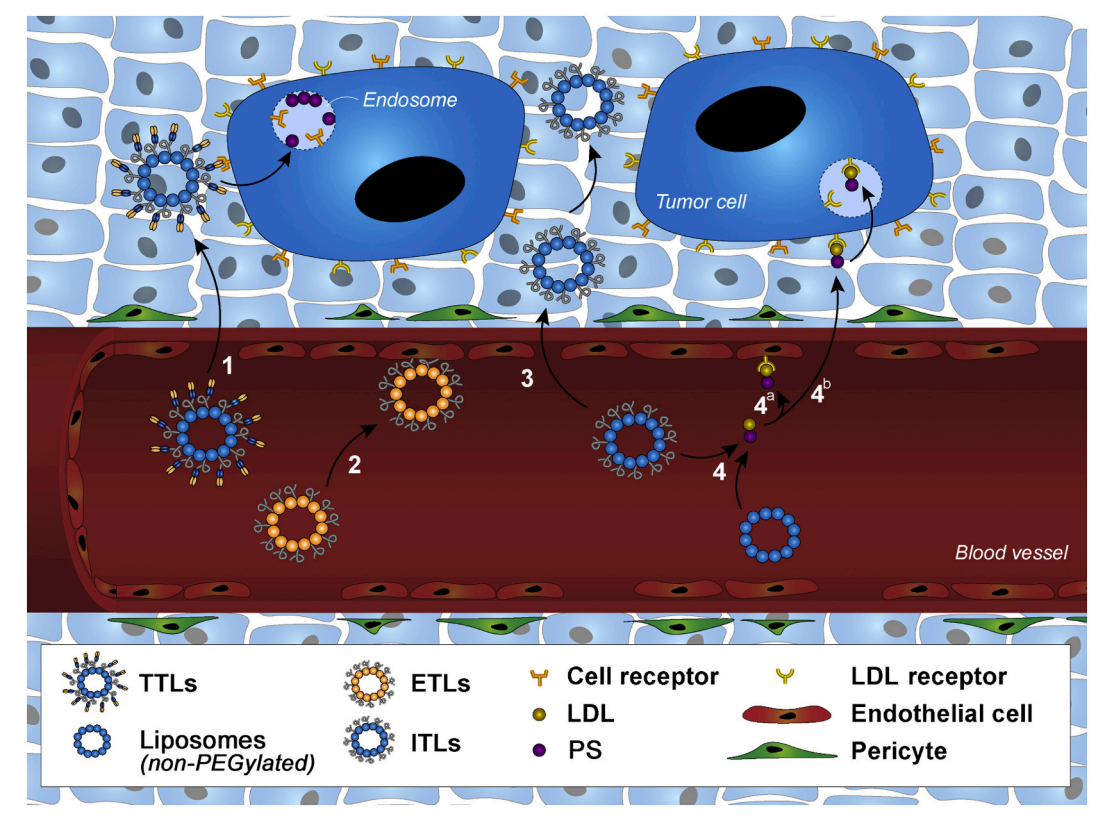


Fig. 2. Multi-targeted photonanomedicines platform for photodynamic therapy (PDT) of solid tumors. Photosensitizer (PS) molecules can be delivered to key tumor anatomical sites *via* 4 delivery routes, designated 1–4. For photosensitization of parenchymal cells (route 1), tumor cell-targeting liposomes (TTLs) can be used that are decorated with surface protein recognition domains (*e.g.*, nanobodies) designed against proteins that are overexpressed on tumor cells. Following extravasation through inter-endothelial gaps in the tumor vasculature, the TTLs bind to the cognate ligand and are subsequently internalized to deliver the PS cargo. PDT of TTL-delivered PS results in tumor cell death. Similarly, the tumor vasculature can be photosensitized using endothelium-targeting liposomes (ETLs; route 2), which are PS-encapsulating PEGylated cationic liposomes. The positive charge of the liposome surface leads to preferential association with the overly negative charge of the tumor endothelial glycocalyx, leading to liposomal uptake [19] and PS delivery. PDT of ETL-delivered PS results in vascular occlusion and tumor cell death due to anoxia and nutritional deprivation. The tumor microenvironment can be photosensitized by passive diffusion of PS-encapsulating PEGylated interstitially targeted liposomes (ITLs) into the stroma (route 3) *via* the enhanced permeability and retention (EPR) effect. PDT of ITL-delivered PS leads to oxidative damage to structural proteins and stromal cells, including resident immune cells. It has also been reported that the PS can be extracted from non-PEGylated ITLs in the circulation by low density lipoprotein (LDL) and delivered to tumor cells following LDL uptake by LDL receptors [41,65,66] (route 4). PDT of LDL-delivered PS leads to endothelial damage (thrombosis, vascular shutdown) and parenchymal damage (tumor cell death).

cellular constituents of the tumor microenvironment [77–79] and vascular shutdown [28,80–83] is, in the broader context of PDT, considered a secondary phenomenon with largely an adjuvant contribution to PDT outcome.

Accordingly, uptake of ZnPC-ITLs, ZnPCS4, AlPC-ITLs, and AlPCS4 by tumor cells in addition to photosensitizing the tumor stroma and interstitial space would be beneficial to PDT efficacy and negates the necessity of co-administering TTLs. The TTLs are more difficult to massproduce under GMP conditions and are also considerably more costly due to the use of biologicals (i.e., nanobodies). Coincidentally, despite PEGylation and non-association of ITLs with certain blood cells [21,84], ZnPC-ITLs were found to be taken up by and photosensitize tumor cells [9,11] and therefore inherently possess multi-targeting properties, which may be advantageous to therapeutic efficacy. How the dark toxicity, uptake kinetics, intracellular distribution, and phototoxicity of ZnPC-ITLs compare to those of ZnPCS4, AlPC-ITLs, and AlPCS4 is currently elusive yet important to understand in a PS selection trajectory with clinical implementation as final aim. These parameters were therefore investigated by stepwise attrition in human epidermoid carcinoma (A431) cells to arrive at the most suitable PSs for PC-based PDT.

A431 cells were used because (1) these cells have a dysfunctional *P53* tumor suppressor gene [85] – a feature shared by a plethora of cancers [86] – and (2) the cells overexpress epidermal growth factor receptor (EGFR) [87], which is a metabolically important receptor in many tumors [88] and is downregulated by PDT [26,89]. A431 cells therefore act as a generic test system that could be extended to spin-off PDT studies with specific cancer types.

3.2. Liposomal Phthalocyanines Are Not Cytotoxic up to 1.5 μ M, while Tetrasulfonated Phthalocyanines Induce Mild-to-Moderate Dark Toxicity at Concentrations of \geq 2.5 μ M

In the absence of light, the PSs should not confer any toxicity [5]. In a PS attrition approach, the manifestation of dark toxicity therefore constitutes a first-step measure that could signal the discontinuation of a PS. Accordingly, PS concentration-dependent and clinically relevant incubation time-dependent dark toxicity were determined with the WST-1 assay, given the preferential localization of ZnPC and AlPC to mitochondrial membranes [90,91]. Analysis of the mitochondrial redox state was ensued by the SRB assay of the same cell culture as a robust method for general cell death [57]. DMSO (20%) was used as positive control for complete cell death and DMEM $^{-/-}$ as negative control.

Without photoactivation, the ZnPC-ITLs (122 ± 1 nm, PDI = 0.49 ± 0.02 , ζ -potential = -10.1 ± 1.1 mV; Fig. S1) and AlPC-ITLs (173 ± 7 nm, PDI = 0.68 ± 0.02 , ζ -potential = -9.6 ± 1.1 mV; Fig. S1) did not induce notable A431 cell death up to a PS concentration of $1.5\,\mu\text{M}$, equating to 500- μ M final lipid concentration (Fig. 3). This PS and lipid concentration range had been employed in previous work on ZnPC-ITLs [9,11] with comparable results. Dark incubation of cholangiocarcinoma (Sk-Cha1) cells with ZnPC-ITLs at $1.5\,\mu\text{M}$:500 μ M PS:lipid concentration produced no dark toxicity [9,11]. In toxicogenomics investigations, none of >40,000 analyzed gene transcripts were dysregulated in Sk-Cha1 cells at these ZnPC and lipid concentrations compared to buffer control [11], underpinning the non-toxicity of ZnPC as well as the ITLs in the absence of light. The results were reproducible for AlPC-ITLs in A431 cells with both cell viability assays.

ZnPCS4 and AlPCS4 exhibited moderate (up to 30% cell death) and mild (up to 10% cell death) dark toxicity in A431 cells, respectively, that was concentration-dependent but not incubation time-dependent (Fig. 3B). As opposed to the lipophilic PS, the tetrasulfonated species mainly occupy the cytoplasm and are excluded from mitochondria [92]. In line with this localization pattern, cytotoxicity was revealed through the SRB assay but not the WST-1 assay. Contrastingly, Qualls et al. [92] reported no dark toxicity of AlPCS4 in human nasopharyngeal carcinoma (KB) cells following 4-h loading of up to 2.5 mM AlPCS4 and subsequent 48-h incubation. Similarly, no dark toxicity (LC50 > 100 μ M)

was observed for ZnPCS4 in human mammary carcinoma (MCF-7) cells, human oral squamous cell carcinoma (HSC-2) cells, and human colorectal carcinoma (HCT 116) cells [39], altogether indicating that the sensitivity to the tetrasulfonated PCs is cancer cell line-dependent. Neither ZnPCS4 nor AlPCS4 exhibited toxicity at the highest tested concentration of ZnPC and AlPC (1.5 μ M) in A431 cells.

3.3. Liposomal and Tetrasulfonated Metallated Phthalocyanines Are Taken up by Cancer Cells and Rapidly Disperse to Multiple (Intra)Cellular Loci

A compound can only exert cytotoxic effects if it associates with cells and is internalized. In the second attrition step, the association, internalization, and intracellular distribution of the PSs with cells were assayed by flow cytometry and confocal microscopy, respectively, using the intrinsic fluorescence properties of the metallated PCs (Fig. S2). Inasmuch as the molar extinction coefficient, fluorescence quantum yield, molar absorptivity at 671 nm, and fluorescence lifetime differ among the PSs [6,93,94] the fluorescence intensity cannot be used for intergroup comparison, but only intragroup analysis to e.g., monitor changes over time.

Flow cytometry revealed that all PSs associated with cells within 1 min of interaction and that the PS-cell interaction became more profuse with incubation time (Fig. 4A). All PSs entered the tumor cells and gradually distributed throughout the cells over the course of 1 h without entering the nucleus (Fig. 4B).

The current results regarding PC-ITLs corroborate our previous findings that ITLs are taken up by cultured human cholangiocarcinoma (Sk-Cha1) cells and therefore - at that time assumingly - deliver lipophilic PC molecules into the cell [9]. In those prior studies we employed the lipophilic tracer rhodamine-PE as PC mimetic and observed its distribution across the cell and organelles (mitochondria) during 4-h incubation by fluorescence microscopy. Corroboratively, the uptake of different non-targeted liposomes has also been reported for other cancer cell lines by other research groups [90,95]. From previous work [9,90,95] together with the confocal microscopy data (Fig. 4B) it can be concluded that the entire macromolecular complex is internalized by cells, after which the individual components scatter to different subcellular loci [17]. ITL uptake by A431 cells was not facilitated by proteins adsorbed to the liposome surface [96], as the ITLs were added to medium that was not supplemented with FBS or proteinaceous constituents. PEGylation did not impair cell entry, nor did it notably interfere with uptake dynamics (Fig. 4A), particularly when the intracellular ZnPC fluorescence pattern of PEGylated ZnPC-encapsulating liposomes (this study) is juxtaposed to that of ZnPC delivered into transformed rat embryo (4R) fibroblasts by non-PEGylated liposomes (ZnPC-liposomes from Ciba-Geigy composed of POPC and OOPS at a 9:1 w/w ratio) [90].

The intracellular distribution of ITL-delivered ZnPC occurred at a slower rate than ITL-delivered AIPC (Fig. 4B) despite an equal degree of PEGylation and liposomal membrane surface properties, which govern nanoparticle-cell interactions in our test system [95]. Apparently, the central coordinated metal in phthalocyanines not only dictates photophysical and photochemical properties of phthalocyanines [94,97-99] but also their intracellular distribution kinetics following liposomal delivery. Changes in localization are well-documented for PS that have been covalently modified with functional groups [100], but not per se as a result of coordinated metal substitution. The dissimilar distribution kinetics between ZnPC and AlPC are reflected in the differential compartmentalization in the early stages of ITL-cell interactions. After 15-min incubation, ZnPC mainly accumulated in the outer membrane (Fig. 4B, yellow arrows) and progressively populated intracellular sites. AIPC did not exhibit an initial accumulation in the cell membrane but rapidly dispersed throughout the cell via intracellular vesicles (Fig. 4B, yellow arrow). After 60-min incubation the intracellular presence and distribution of ZnPC and AlPC were mostly comparable. Both PCs photosensitized numerous (intra)cellular loci that are known to include the

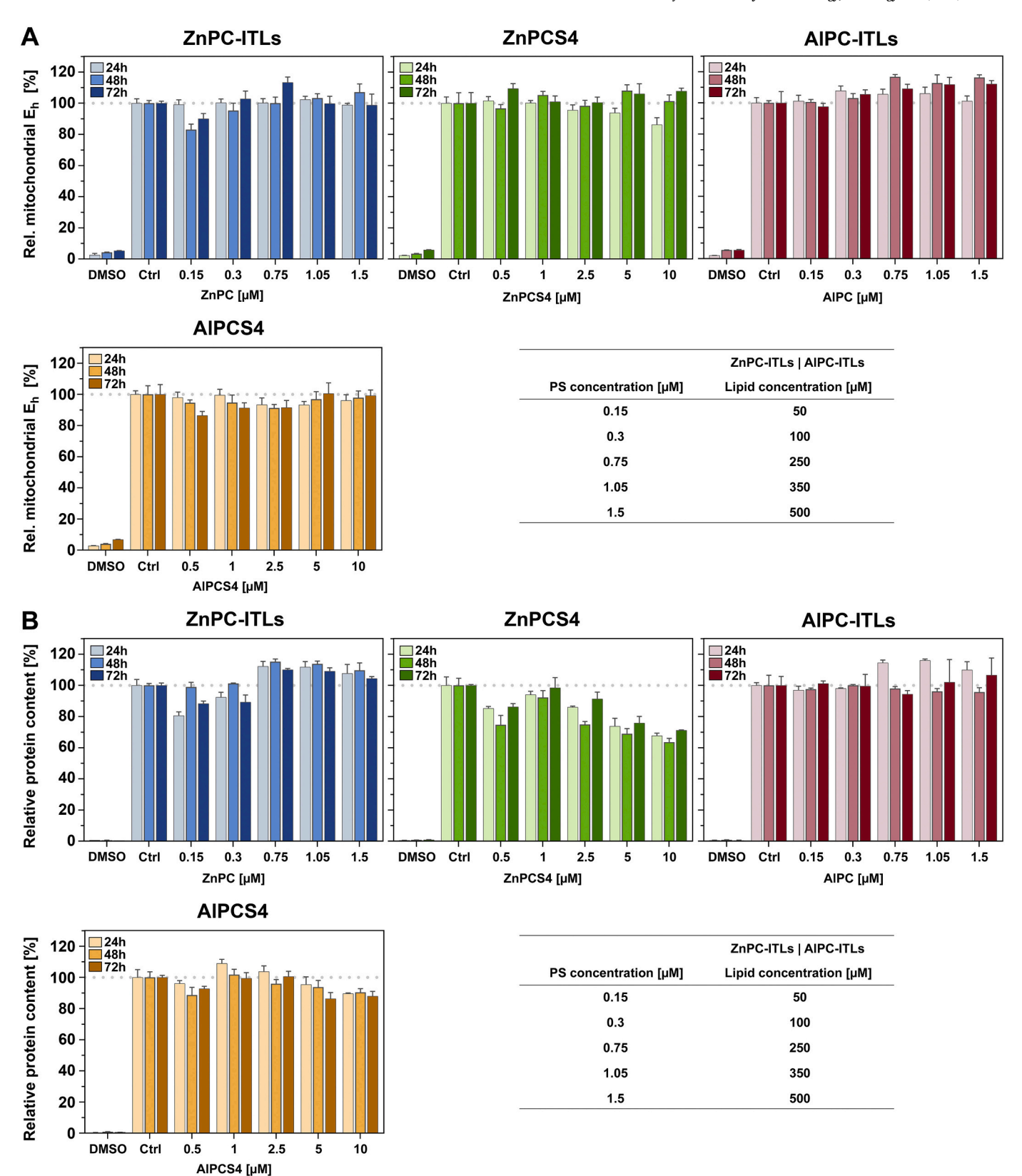


Fig. 3. In vitro dark toxicity. A431 cells were incubated with AlPC-ITLs and ZnPC-ITLs (0–1.5 μM final concentration) and AlPCS4 and ZnPCS4 (0–10 μM final concentration) in DMEM $^{-/-}$ and maintained under standard culture conditions for 24 h, 48 h, and 72 h. Cell were assayed by WST-1 for mitochondrial redox state (A) and by SRB for total protein content (B), both used as indicator of cell viability. Positive control comprised 20% DMSO in DMEM $^{-/-}$ while the negative control was DMEM $^{-/-}$. Data (N=3 per concentration per time point) were normalized to the control group mean. The tables provide the final lipid concentration of ITLs per photosensitizer concentration, all at a photosensitizer:lipid molar ratio of 0.003. Abbreviations: AlPC, aluminum phthalocyanine; AlPCS4, tetrasulfonated aluminum phthalocyanine; E_h, redox potential; ITLs, interstitially targeted liposomes; PS, photosensitizer; Rel., relative; ZnPC, zinc phthalocyanine; ZnPCS4, tetrasulfonated zinc phthalocyanine.

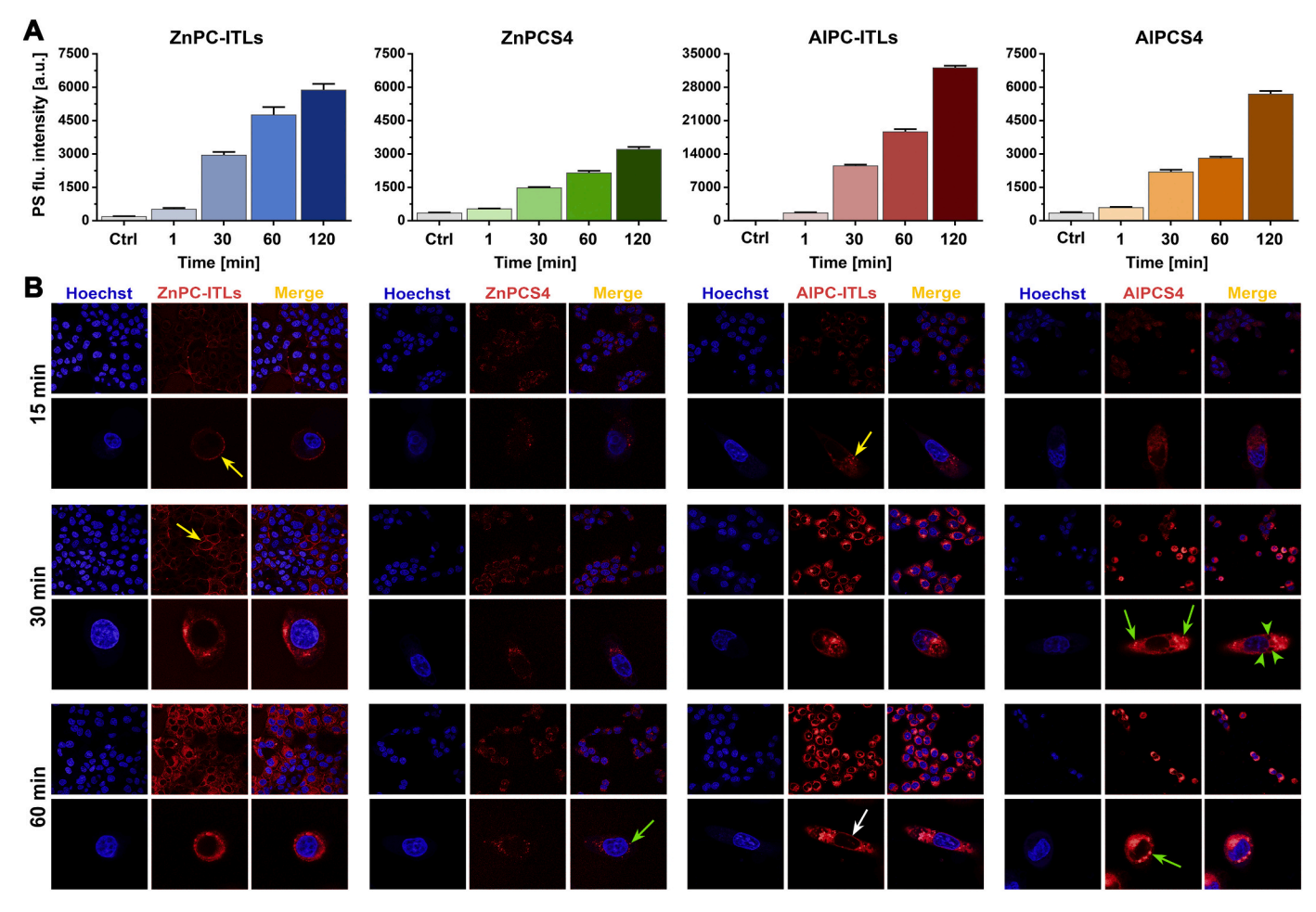


Fig. 4. Uptake and intracellular distribution of native and tetrasulfonated zinc- and aluminum phthalocyanine in A431 cells. (A) A431 cells were incubated with 0.375 μM of photosensitizer (PS) in DMEM $^{-/-}$ for 1–120 min and analyzed by flow cytometry. The mean PS autofluorescence intensity is plotted as a function of incubation time (N = 3 per time point). (B) A431 cells were incubated with AlPC-ITLs and ZnPC-ITLs (3 μM PS concentration, 1000 μM lipid concentration) and AlPCS4 and ZnPCS4 (10 μM) for 15–60 min and imaged by confocal microscopy (red fluorescence). Hoechst 33342 (blue fluorescence) was used to stain DNA. The yellow arrows designate photosensitizer accumulation in the cell membrane (ZnPC) and intracellular dispersion via vesicular trafficking (AlPC). The white arrow points to perinuclear accumulation of ITL-delivered AlPC. The green arrows point to hyperfluorescent compartmentalized ZnPCS4 and AlPCS4. The green arrowheads indicate perinuclear compartments devoid of AlPCS4. Additional exemplary images are provided in Fig. S3. Abbreviations: AlPC, aluminum phthalocyanine; AlPCS4, tetrasulfonated aluminum phthalocyanine; flu., fluorescence; ITLs, interstitially targeted liposomes; PS, photosensitizer; ZnPC, zinc phthalocyanine; ZnPCS4, tetrasulfonated zinc phthalocyanine.

membranes of mitochondria, endoplasmic reticulum, Golgi apparatus, and lysosomes [51,90,101]. AlPC also localized to or at the nuclear membrane at 60-min incubation (Fig. 4B, white arrow) while ZnPC did not. More detailed examples of the differential intracellular localization of the PSs are provided in Fig. S3.

The differential uptake kinetics of ZnPC and AlPC over the course of 1 h are rather inconsequential to clinical PDT outcomes relative to the employed drug-light intervals, that are generally in the order of 1-2 days. Intracellular localization, on the other hand, is not trivial in clinical context insofar as nuclear membrane photosensitization may contribute to additional or preferential modes of cell death that could account for more profound phototoxicity and/or anti-tumor immune response, respectively [6].

The association profile of ZnPCS4 and AlPCS4 with A431 cells was comparable to that of ITL-delivered ZnPC and AlPC, respectively. Intracellular fluorescence of tetrasulfonated ZnPC and AlPC increased over time and did not reach saturation over the course of 1 h (Fig. 4A). In contrast to the parent compounds, AlPCS4 did not exhibit such profound compartmentalization initially, although fluorescent clusters were observed at longer incubation times (30 min and beyond) (Fig. 4B, green arrows). Instead, AlPCS4 distributed more homogenously throughout

the entire cell except the nucleus and some perinuclear compartments (Fig. 4B, green arrowheads). Similar intracellular distribution patterns have been observed for AlPCS in Chinese hamster lung (V-79) fibroblasts (24-h incubation, 50 μ M), where the extent of internalization and hence photosensitization was reliant on the degree of sulfonation and proceeded in the order of tetrasulfonated > trisulfonated > disulfonated [102]. Compartmentalized AlPCS4 was also observed in KB cells following 4-h incubation at 12.5-μM PS concentration [92]. Intracellular localization of ZnPCS4 was more difficult to assess by confocal microscopy due to the debilitating effect of the Zn atom on PC fluorescence quantum yield and fluorescence lifetime [94,97-99] (Fig. 4B). Despite the hampered fluorescence intensity, the distribution pattern suggested early onset compartmentalization of ZnPCS4 (Fig. 4B, green arrows) in what are most likely lysosomes, given the strong negative charge of ZnPCS4 in combination with the near-immediate manifestation of clustering (Fig. 4B) [6,100,103].

The confocal microscopy results attest to the possibility to guide intracellular PC localization by the chemical composition of the PC, if intracellular delivery *in vivo* is successful. Photosensitization of specific intracellular loci is generally reserved for individual classes of PSs [6]. For example, ALA can be used to photosensitize mitochondria after

conversion to protoporphyrin IX [104,105]. Temoporfin (mTHPC) exhibits a preference for the endoplasmic reticulum and Golgi apparatus [106]. Porfimer sodium chiefly localizes to the cell membrane and Golgi apparatus [107], while anionic PSs mostly end up in lysosomes

[100,103].

Damage to each subcellular structure triggers its unique cell death signaling cascade(s) [108]; intracellular PS localization is therefore important for therapeutic efficacy and outcome. Based on the confocal

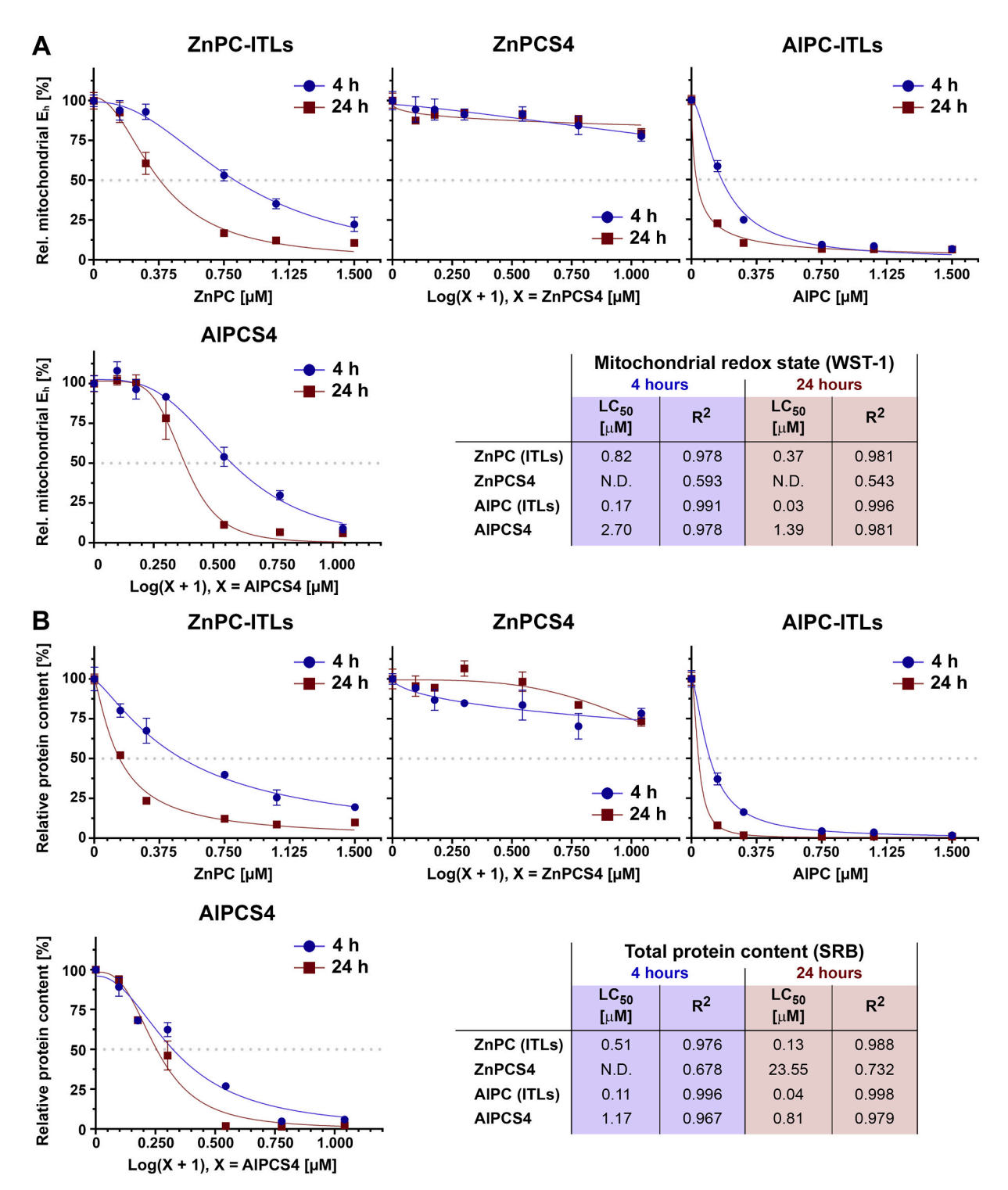


Fig. 5. PDT-induced cell death as a function of photosensitizer (PS) concentration and incubation time. A431 cells were incubated for 1 h with ZnPC-ITLs, ZnPCS4, AlPC-ITLs, and AlPCS4 and washed directly before PDT (cumulative radiant exposure of 15 J/cm²). Cell viability was assessed by the WST-1 assay (mitochondrial redox potential (E_h)) (A) and by the SRB assay (total protein content) (B) at 4 h and 24 h post-PDT (N=3 per PS concentration per incubation time). PS incubation and post-PDT recovery were performed in DMEM $^{-/-}$ under standard culture conditions. Results were normalized to the mean value of the control group (medium only, cumulative radiant exposure of 15 J/cm²). Fits were generated using the non-linear fit data analysis function in GraphPad Prism, from which the median lethal PS concentration (LC_{50}) was calculated. The goodness of fit (R^2) value is provided for each fit. Abbreviations: AlPC, aluminum phthalocyanine; AlPCS4, tetrasulfonated aluminum phthalocyanine; ITLs, interstitially targeted liposomes; PS, photosensitizer; SRB, sulforhodamine B; WST-1, water-soluble tetrazolium 1; ZnPC, zinc phthalocyanine; ZnPCS4, tetrasulfonated zinc phthalocyanine; N.D., not determined.

imaging, PCs can be directed to important intracellular sites by selecting the appropriate coordinated metal [109] and by employing tetrasulfonated derivatives, which are also commercially available, at least for ZnPC and AlPC. Accordingly, using multiple metallated PC(S4)s in a single PS delivery platform is expected to lead to more comprehensive photosensitization of tumor cells and consequently the photochemical activation of various critical modes of cell death (necrosis, apoptosis, necroptosis, and autophagy) upon PDT [6,100,103]. It should be noted that most cell death pathways may diverge to necrotic cell death in vivo [6,100,103,110] when these concur with vascular shutdown-mediated hypoxia [58,59,111-113] (i.e., ATP depletion [114]) and metabolic catastrophe (i.e., ceased nutrient supply [115] and ATP production [26]), which both favor necrosis [108]. In any respect, the PS delivery platform illustrated in Fig. 2 can be further finetuned by incorporating multiple metallated PCs and sulfonated derivatives for a comprehensive approach to photochemical cell death induction.

3.4. Aluminum-Based Phthalocyanines Are more Phototoxic than Zinc-Based Phthalocyanines

The extent to which each light-exposed PS kills cancer cells constituted the next step in the attrition procedure. A431 cells were photosensitized at increasing PS concentration and the LC50 was calculated from the concentration-effect fitted curve functions as a measure of cell phototoxicity and PDT efficacy. Inter-PS differences between the Q-band absorption maximum of ZnPC, AlPC, and AlPCS4 (Figs. 1 and S2) and the laser wavelength (671 nm) were discounted. The decrease in molar extinction coefficient, and hence the extent of ROS generation, due to a mismatch between the Q-band maximum and laser line was deemed too small to produce significant differences in outcome (i.e., differences that would not exceed the standard deviation). For ZnPCS4, the absorption of 671-nm light is about 40% of that at the absorption maximum, translating to a molar absorptivity ($\epsilon = 118,000$) that approximates the molar absorptivity of AlPC ($\epsilon=126{,}000)$ and AlPCS4 ($\epsilon=158{,}000)$ at their absorption maximum (Fig. 1), which is near the 671-nm laser wavelength. At published triplet state quantum yields of 0.47, 0.41, and 0.38 of ZnPCS4, AlPC, and AlPCS4, respectively, and singlet oxygen (¹O₂) quantum yields of 0.43, 0.34, and 0.38, respectively (Fig. 1), the amount of ROS produced by ZnPCS4 should theoretically not veer much from the amount of ROS produced by the Al-based PSs. In light of the intracellular distribution pattern (Fig. 4B), the aforementioned photophysical and photochemical properties, and experimental data, it was expected that phototoxicity would be most eminent for the ITL-delivered lipophilic PCs and proceed in the order of ZnPC-ITLs > AlPC-ITLs > AlPCS4 > > ZnPCS4. The (peri)nuclear localization of AlPC observed in this study (Fig. 4B) and the unexpectedly more overwhelming fluorogenic redox probe oxidation by AIPC versus ZnPC in physiological buffer published previously [6] could narrow or even tilt the phototoxicity in favor of

Indeed, ITL-delivered AlPC was most phototoxic to A431 cells as evidenced by the LC_{50} values for both read-out parameters, which were in the low-nanomolar range (Fig. 5). The LC_{50} values for ZnPC-ITLs were 5-fold (4 h post-PDT) and 3–10-fold higher (24 h post-PDT) compared to AlPC-ITLs. The LC_{50} could not be calculated for ZnPCS4, making the phototoxicity order AlPC-ITLs > ZnPC-ITLs > AlPCS4 >> ZnPCS4. The cellular phototoxicity of the photosensitizers mimics their ROS-generating capacity reported earlier [6]. The fact that the degree of lethality was exacerbated for all PSs except ZnPCS4 at 24 h post-PDT compared to 4 h post-PDT indicates that the execution of cell death pathways predominated over any survival signaling [11,26,64], damage remediation, and salvage mechanisms. We could not confirm the utility of ZnPCS4 in PDT of A431 cells as reported previously for other cell types [28,29,32].

The pleiotropic photosensitization pattern of lipophilic metallated PCs (Fig. 4B) seems to be advantageous to photokilling efficacy (Fig. 5), as was expected for membrane-targeting PSs and the lethality of multi-

site-targeted PSs [74]. PCs such as ZnPC produce ROS via type I (superoxide anion, hydroxyl radical (\bullet OH), and hydrogen peroxide) [116] and type II photochemical reactions (1O_2) [117,118]. 1O_2 has a very short half-life (< 40 ns) in a biological milieu [119] because of its extreme reactivity towards lipids, proteins, and nucleic acids [120,121]. The same applies to \bullet OH [122,123], whose reactivity is so high that the reaction rate constants towards organic biomolecules [124] approximate the diffusion-controlled limit in aqueous solution [125]. Accordingly, both ROS have a narrow action radius [119,125] and inflict deleterious redox modifications proximal to their production site [9,126].

Photogeneration of ROS in cellular and subcellular membranes, where phospholipids consequently undergo peroxidation by ¹O₂ [127] and •OH-induced radical chain-propagated oxidation [128], has lethal consequences on membrane function and (sub)cellular homeostasis [129]. Oxidation of membrane constituents results in increased barrier permeability and leakage of content [9,130], loss of mitochondrial membrane potential, and disruption of membrane-associated signaling systems [114,131]; i.e., precursor events to various forms of cell death [132,133]. ROS produced by lipophilic PCs also oxidatively modify (transmembrane) proteins and deregulate vital systems in cell metabolism, damage remediation, and proliferation [26,134]. Ergo, when local PDT-induced hyperoxidative stress culminates in (1) metabolic catastrophe (redox damage to mitochondria); (2) the cell's inability to resolve the stress due to impaired protein and lipid synthesis (redox damage to the endoplasmic reticulum), and (3) hampered posttranslational modifications to proteins and protein trafficking (redox damage to the Golgi apparatus), cell death signals are triggered that result in a mix of predominantly apoptosis and necrosis [9,10,17,62,135]. Leakage of lysosomal content (redox damage to lysosomes) (4) will further amplify the cell death signaling [136].

The results in Fig. 5 demonstrate that, at equimolar concentrations, photosensitization of most lipophilic subcellular compartments by ZnPC and AlPC translates to more cell death upon PDT than photosensitization of cytosolic regions and lysosomes by AlPCS4. As per attrition scheme, the multi-targeted photonanomedicines platform (Fig. 2) would benefit most from AlPC compared to the other tested metallated PCs. Theoretically, equal tumoricidal effects could be realized with lower AlPC-ITL dosages compared to ZnPC-ITLs, which aligns with the aim to augment therapeutic efficacy while minimizing photoallergic skin reactions. To date we have been developing the PS delivery platform using ZnPC [9–12,17,18,26,62]. Future research efforts will therefore be directed at head-to-head analysis of liposomal AlPC *versus* liposomal ZnPC with respect to *in vivo* skin phototoxicity, systemic toxicity, intratumoral PS accumulation, and PDT efficacy.

3.5. PDT of A431 Cells Leads to a Mixed Mode of Cell Death Dominated by Apoptosis and Cell Cycle Arrest

PDT can destroy tumors by vascular shutdown [28,58,59,80-83], immunological cell death [137], and direct tumor cell death [74]. Direct photokilling practically translates to in situ tumor debulking and prevents tumor cells from recovering via survival signaling [64,138], the relevance of which has been attested in vitro [11,26,139], in vivo [140], and in the clinical setting [141]. PDT triggers different modes of cell death that include necroptosis (programmed necrosis), secondary necrosis (apoptosis turned into necrosis, also referred to as late apoptosis), paraptosis, and apoptosis (especially due to ER stress) [74,133,142,143]. When irreparable damage occurs in the form of mitochondrial dysfunction, cell membrane damage, oxidative stress, and release of lysosomal enzymes [144], the abovementioned cell death programs generally execute and converge to a phenotype where phosphatidylserine is exposed on the outer membrane leaflet and/or the cell membrane becomes permeable [145,146]. Correspondingly, these hallmark events were measured by flow cytometry following annexin V and propidium iodide staining and stratified into healthy cells (annexin

 $V^{-/-}/PI^{-/-}$), early apoptotic (annexin $V^{+/+}/PI^{-/-}$), late apoptotic (annexin $V^{+/+}/PI^{+/+}$), and necrotic cells (annexin $V^{-/-}/PI^{+/+}$) [60].

In the first set of experiments, cells were incubated with increasing PS concentration for 1 h, subjected to PDT, and assayed by flow cytometry 4 h after treatment (Fig. 6A). The supernatant containing detached cells as well as the harvested cells were pooled for analysis. In line with the WST-1 and SRB data (Fig. 5), cells that had been incubated with ZnPCS4 did not exhibit notable apoptotic or necrotic features at concentrations up to $5 \mu M$. In other studies, substantially higher ZnPCS4 concentrations (IC50 and IC75 of 216 μM and 500 μM , respectively, in human cervical cancer (SiHa) cells) were required to achieve mainly necrotic cell death [147]. However, photomedicines requiring such high concentrations are clinically not warranted or worth investigating further when superior PSs such as AlPC, ZnPC, and AlPCS4 are available. The liposomal PSs induced a mixed set of cell death modes where early apoptosis prevailed at the lower PS concentration (0.15 µM) while late apoptosis predominated at the higher PS concentration (1.5 µM). Necrosis was observed in 1-2% of the cells that had been photosensitized with ZnPC-ITLs and AlPC-ITLs at 0.75 and 1.5 μ M PS concentration. In contrast, AlPCS4 at 0.75 μ M induced early apoptosis, late apoptosis, and necrosis at an approximate ratio of 2:3:1. The fraction of early apoptotic cells did not change much at higher AlPCS4 concentrations, only the percentage of necrotic cells at the expense of late apoptotic cells.

An obvious difference between the hydrophilic AlPCS4 and ITL-delivered lipophilic AlPC was the extent of necrotic cell death that had manifested as early as 4 h after PDT. At 2.5 μM AlPCS4, which equates to the 4 h post-PDT LC50 value as determined by the WST-1 assay (Fig. 5A), there was 84% total cell death, of which $16\pm10\%$ was attributable to necrosis (Fig. 6A). This contrasts with the 25% total cell death and merely $1\pm0\%$ necrosis induced by liposomal AlPC at the near-LC50 concentration of 0.15 μM at the same time interval (Fig. 6A versus Fig. 5A). We subsequently looked into post-PDT energy metabolism as a possible explanation, given that necrosis is an ATP depletion-depend phenomenon while apoptotic programs require energy [148]. Ndhundhuma and Abrahamse [149] reported that human melanoma (A375) cells photosensitized with AlPCS4 (2.5 μM) and illuminated at a

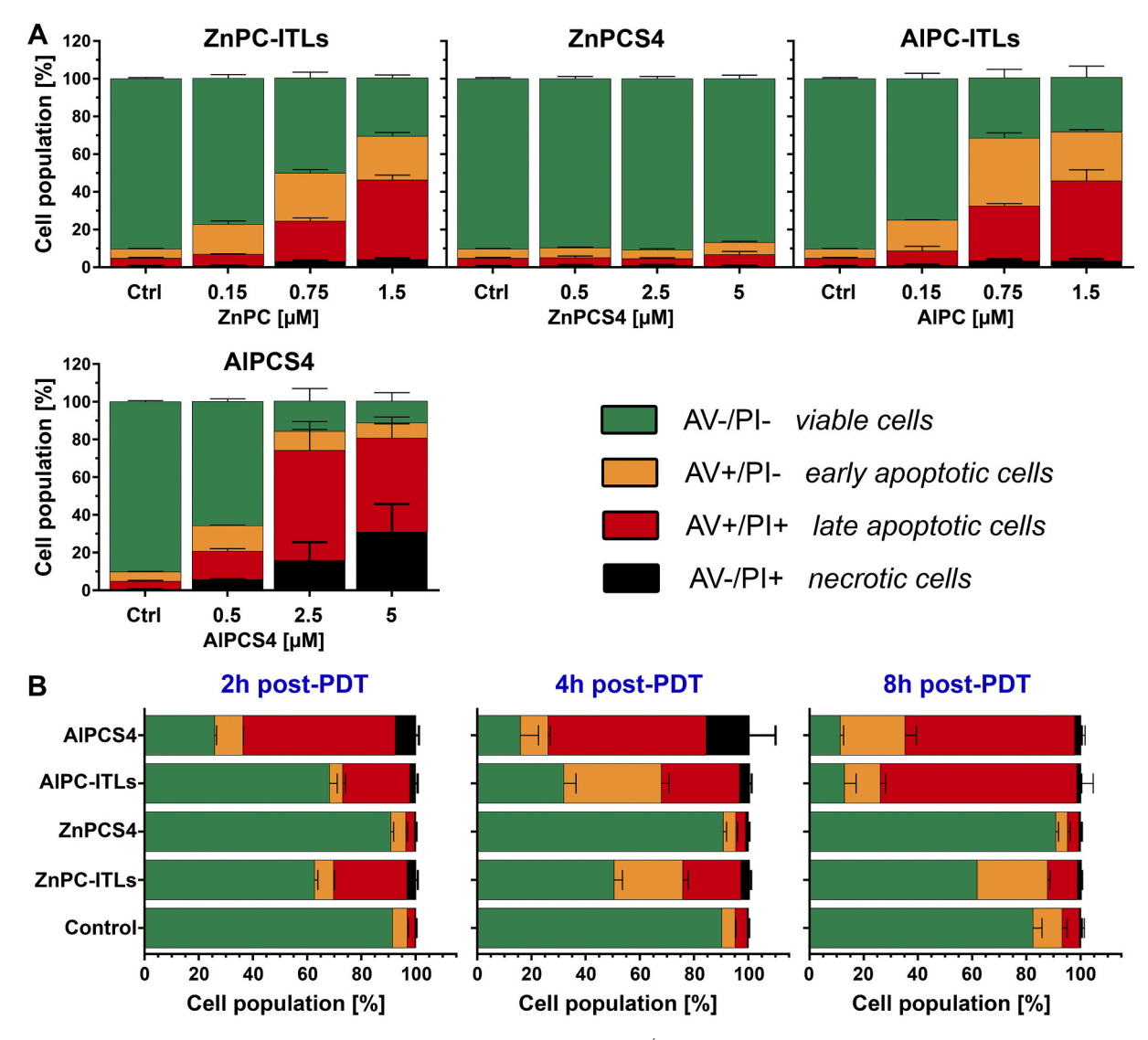


Fig. 6. Mode of cell death induced by PDT. A431 cells were incubated with PS in DMEM $^{-/-}$ for 1 h, washed, treated by PDT (cumulative radiant exposure of 15 J/cm 2) or left untreated (control), and stained with PI and annexin V after incubation in DMEM $^{-/-}$. The mode of cell death was analyzed by flow cytometry of both the supernatant fraction and harvested cells detached by trypsinization. (A) Photosensitizer concentration-dependent mode of cell death at 4 h post-PDT. Values are shown as mean \pm SD for N = 3/group. (B) Mode of cell death evolution during the first 8 h after PDT (ZnPC and AlPC, 0.75 μ M; ZnPCS4 and AlPCS4, 2.5 μ M). Data represent mean \pm SD for N = 3 per photosensitizer concentration and post-PDT incubation time. Abbreviations: AlPC, aluminum phthalocyanine; AlPCS4, tetrasulfonated aluminum phthalocyanine; AV, annexin V; ITLs, interstitially targeted liposomes; PI, propidium iodide; ZnPC, zinc phthalocyanine; ZnPCS4, tetrasulfonated zinc phthalocyanine.

cumulative radiant exposure of 10 J/cm² lost \sim 80% of their baseline ATP levels at 4 h post-PDT. However, only 0.9% of the cells were necrotic, while 9.9% were early-apoptotic and 2.2% were late-apoptotic. In contrast, illumination (15 J/cm²) of human biliary carcinoma (Sk-Cha1) cells photosensitized with ZnPC-ETLs did not lead to significant ATP depletion at 90 min post-PDT [26]. In fact, only a \sim 15% drop in ATP concentration was measured at both LC50 and LC90 despite ample evidence of mitochondrial dysfunction. Both studies were performed with cells that had been exposed to a normoxic atmosphere after PDT, dismissing the possibility that the drop in ATP was caused by hypoxia. The reasons behind the AlPCS4-induced necrosis therefore does not seem to be related to disrupted energy metabolism *per se*. In an ancillary example, Kessel et al. [114] observed loss of mitochondrial membrane potential following PDT and consequent progression of apoptosis, which was incongruous with the depleted intracellular ATP levels.

In the second set of experiments, the mode of cell death was investigated as a function of time after PDT to assess how fast the cell death pathways were executed and to what extent. As presented in Fig. 6B, ZnPCS4 had no effect on cells, whereas AlPCS4 induced the most extensive cell death signaling 2 h after PDT (74%). With time, the percentage of dead/dying cells increased to 84% (4 h) and 89% (8 h). Although AlPC-ITLs inflicted roughly half of the degree of cell death at 2 h post-PDT compared to AlPCS4, at 8 h the fraction of dead/dying cells was comparable (87%), indicating that the progression of cell death signaling occurred at a slower pace for the lipophilic PS. This trend was echoed by ZnPC-ITLs, albeit to a lesser extent (37%, 49%, and 38% at 2 h, 4 h, and 8 h, respectively), which is consistent with the WST-1 and SRB data obtained 4 h post-PDT (Fig. 5). Moreover, the cells in the AlPCS4 group transitioned from a more severe form of cell death (late apoptosis) to a less severe form of cell death (early apoptosis). The same applied to cells in the ZnPC-ITL group, although a reversal in the magnitude of cell death signaling was found during the 4-8 h interval. These trends were absent in cells that had been treated with AIPC-ITLs, which progressed to a more severe cell death profile with time. The time required to count 10,000 cells in the gated region increased with post-PDT time in the AlPC-ITL and AlPCS4 group (Fig. S4A). Also, the amount of cell remnants, microparticles, and debris produced by dying and dead cells increased after PDT for all PSs that induced photokilling compared to control cells (Fig. S4B). The implications of these observations are discussed further in section S3.5 and Figs. S3-5. It should be noted that the observed modes of cell death were most likely not attributable to the inherent toxicity of the PSs (Fig. 3) considering previous dark toxicity results at earlier time points [9] and the fact that no dark toxicity was observed at the used PS concentration after 24-h incubation (Fig. 3).

It is known that cell death signaling constitutes a sliding scale phenomenon where biochemical pro-survival stimuli [11,64] may abrogate the death cascades and cause cells to undergo anastasis (cell survival and recovery through reversal of apoptosis [150]) or other modes of recovery [151–153]. In fact, we reported this exact trend several years ago for human biliary carcinoma (Sk-Cha1) cells treated with ZnPC-ITLs (0.75 μ M; cumulative radiant exposure of 15 J/cm²) and ascribed it to cell survival, despite severely impaired mitochondrial redox capacity [9] (as was the case here too, Fig. 5A). These findings may have implications in translational studies. The mode of tumor cell death influences the post-PDT anti-tumor immune response [154] and abscopal effects [155]. In juxtaposition to direct tumor cell photokilling, immunological cell death is additive and above all quintessential in long-term tumor control [137,156]. Qualified modes of cell death for immunological signaling are necroptosis, secondary necrosis, paraptosis, and apoptosis [146,157-163]. It will therefore be interesting to see whether (1) the reversal of cell death prevails in vivo for the AlPCS4 and ZnPC-ITLs and (2) whether it negatively impacts immunological tumor clearance.

In the final test arm, cells were treated by PDT and assayed for cell cycle arrest by PI staining in combination with flow cytometry at 24 h after PDT. As alluded to above, A431 cells are monoallelic for P53 [85],

a tumor suppressor protein that under certain stress conditions can cause cell cycle arrest in G_1 and G_2 and apoptosis [164]. An R273H missense mutation leads to gain of function in terms of increased propensity of evasion and migration but not increased cell cycle progression and cell survival [165]. Conversely, cells were maintained in $\mathsf{DMEM}^{-/-}$ following PDT to emulate post-PDT malnutrition and metabolic catastrophe [26] following vascular shutdown [28,80–83]. Serum deprivation can cause cell cycle arrest in G_0 [166,167], which we observed in control A431 cells (49.1 \pm 0.3%; Fig. 7) when compared to values reported elsewhere for A431 cells cultured in fully supplemented medium (39–43%) [168]. Taken together, control cells had increased G_0 arrest at baseline due to contrived culture conditions while the P53 gene status in itself was not expected to exacerbate cell cycle arrest and apoptosis.

In line with previous data, PDT of cells that had been incubated with ZnPCS4 resulted in cell cycle profiles that were comparable to control cells (Fig. 7). In contrast, cells that had been photosensitized with ZnPC-ITLs, AlPC-ITLs, and AlPCS4 exhibited a reduction in the percentage of cells in G₀/G₁. Cells treated with AlPCS4 were arrested in the S-phase, suggesting perturbation of tightly controlled replication forks that mediate DNA replication. Cells that had been treated with AlPC-ITLs exhibited both S-phase and G2 arrest, which is in sync with the widespread apoptosis (Fig. 6). The G2 phase is only entered if the DNA replication in the S-phase has proceeded successfully and embodies rapid cell growth and protein synthesis in preparation of division. Cells that had been subjected to ZnPC-ITL PDT also exhibited moderate arrest in the S-phase and G2, but less profoundly than the AlPC-ITLs and therefore in accordance with the mode of cell death data (Fig. 6) and degree of cell death (Fig. 5). The less extensive S-phase and G2 arrest in cells exposed to ZnPC-ITLs compared to the cell cycle fallout at equimolar AIPC concentration infers that AIPC is a more lethal PS capable of inducing downstream events that are more favorable for therapeutic efficacy; i.e., photokilling of tumor cells and possibly more widespread anti-tumor immune responses.

4. Summary and Conclusions

This study entailed a head-to-head comparative analysis of four metallated phtahlocyanines for PDT of solid tumors; a study that hitherto had not been performed before. The study was conducted in an attritional sense to allow selection of the most optimal PS for further development of third- and fourth-generation PSs; i.e., nanoparticulate second-generation PSs and nanoparticulate second-generation PSs coencapsulating inhibitors of tumor cell survival pathways, respectively. AIPC encapsulated in ITLs was concluded to be the superior PS on the basis of: (1) no dark toxicity up to a concentration that was 37-50 times greater than its LC₅₀ value at 24 h post-PDT, (2) an LC₅₀ value that was 3 times lower than that of ZnPC and 20 times lower than that of AlPCS4 (at 24 h), (3) rapid and abundant uptake by tumor cells despite an absence of targeting ligands, (4) heterogeneous dispersion to numerous intracellular loci, and (5) extensive cell death induction by apoptosis that was accompanied by the most profound cell cycle arrest in the S-phase and G2. Research on the ZnPCS4 will be discontinued because it failed the attrition step regarding phototoxicity. Although phototoxic, ZnPC-ITLs were again shown to be associated with anastasis, which will need to be further explored before advancing the research with this formulation to in vivo and clinical stages. Next, the results obtained with AlPC-ITLs and AlPCS4 will be validated in other cancer cell lines as well as in vivo with respect to systemic toxicity and toxicogenomics, skin phototoxicity, tumor photosensitization, and anti-tumor efficacy. Also, the combination of liposomal AIPC and AIPCS4 will be explored as a PS cocktail. This approach is expected to inflict oxidative damage at different subcellular structures and hence produce different modes of cell death and immunological responses that could be beneficial to therapeutic efficacy and long-term tumor control.

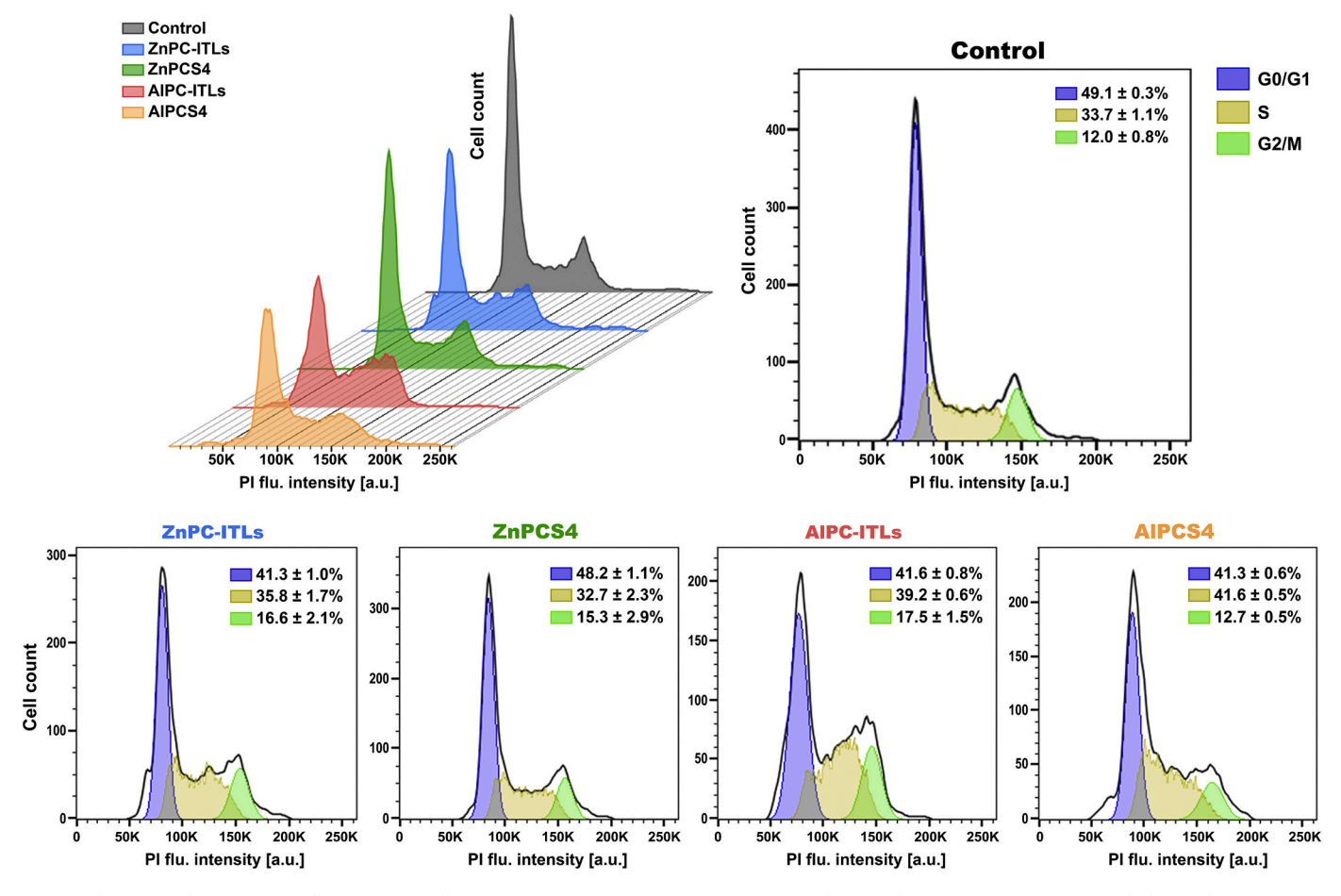


Fig. 7. Cell cycle analysis in A431 cells after PDT. Cells were incubated for 60 min with ZnPC-ITLs, AlPC-ITLs (both 31.25 μM), ZnPCS4, and AlPCS4 (both 0.31 μM), washed, illuminated at a cumulative radiant exposure of 15 J/cm², and harvested 24 h after PDT. Cells were washed twice and PI staining solution and RNAse A in PBS were added after fixation in ice-cold 96% ethanol. Analysis was performed by flow cytometry in the tumor cell gated region. Quantitative data represent mean \pm SD for N = 3/group.

Declaration of Competing Interest

The authors declare that they have no known competing financial interests or personal relationships that could have appeared to influence the work reported in this paper.

Acknowledgements

This work was supported by grants from the Dutch Cancer Foundation (KWF project # 10666), a Zhejiang Provincial Foreign Expert Program Grant, Zhejiang Provincial Key Natural Science Foundation of China (#Z20H160031), and a grant for the establishment of the Jiaxing Key Laboratory for Photonanomedicine and Experimental Therapeutics to MH. BD is sponsored by grants from the National Natural Science Foundation (81872220), a Basic Public Welfare Research Project of Zhejiang Province (LGF18H160034), and the Tumor Nanotargeting and TCM Technology Innovation Team (Key Science and Technology Innovation Team of Jiaxing, 2018). WP is sponsored by a grant from the National Natural Science Foundation of China (31871402). MH is chief formulation officer at Nurish.Me and Camelina Sun and has equity in those companies (whose business activities are unrelated to the present work).

Appendix A. Supplementary data

Supplementary data to this article can be found online at $\frac{\text{https:}}{\text{doi.}}$ org/10.1016/j.jphotobiol.2021.112146.

References

- R. Baskaran, J. Lee, S.G. Yang, Clinical development of photodynamic agents and therapeutic applications, Biomater. Res. 22 (2018) 25.
- [2] G. Shafirstein, A. Battoo, K. Harris, H. Baumann, S.O. Gollnick, J. Lindenmann, C. E. Nwogu, Photodynamic therapy of non-small cell lung cancer. Narrative review and future directions, Ann. Am. Thorac. Soc. 13 (2) (2016) 265–275.
- [3] J.C. Kennedy, R.H. Pottier, D.C. Pross, Photodynamic therapy with endogenous protoporphyrin IX: basic principles and present clinical experience, J. Photochem. Photobiol. B 6 (1–2) (1990) 143–148.
- [4] I.B. Tan, G. Dolivet, P. Ceruse, V. Vander Poorten, G. Roest, W. Rauschning, Temoporfin-mediated photodynamic therapy in patients with advanced, incurable head and neck cancer: a multicenter study, Head Neck 32 (12) (2010) 1597–1604.
- [5] A.P. Castano, T.N. Demidova, M.R. Hamblin, Mechanisms in photodynamic therapy: part one-photosensitizers, photochemistry and cellular localization, Photodiagn. Photodyn. Ther. 1 (4) (2004) 279–293.
- [6] R. Weijer, M. Broekgaarden, M. Kos, R. van Vught, E.A. Rauws, E.J. Breukink, T. M. van Gulik, G. Storm, M. Heger, Enhancing photodynamic therapy of refractory solid cancers: Combining second-generation photosensitizers with multi-targeted liposomal delivery, J. Photochem. Photobiol. C 23 (2015) 103–131.
- [7] M.T. Huggett, M. Jermyn, A. Gillams, R. Illing, S. Mosse, M. Novelli, E. Kent, S. G. Bown, T. Hasan, B.W. Pogue, et al., Phase I/II study of verteporfin photodynamic therapy in locally advanced pancreatic cancer, Br. J. Cancer 110 (7) (2014) 1698–1704.
- [8] Y.J. Shen, J. Cao, F. Sun, X.L. Cai, M.M. Li, N.N. Zheng, C.Y. Qu, Y. Zhang, F. Shen, M. Zhou, et al., Effect of photodynamic therapy with (17R,18R)-2-(1-hexyloxyethyl)-2-devinyl chlorine E6 trisodium salt on pancreatic cancer cells in vitro and in vivo, World J. Gastroenterol. 24 (46) (2018) 5246–5258.
- [9] M. Broekgaarden, A.I. de Kroon, T.M. Gulik, M. Heger, Development and in vitro proof-of-concept of interstitially targeted zinc-phthalocyanine liposomes for photodynamic therapy, Curr. Med. Chem. 21 (3) (2014) 377–391.
- [10] R. Weijer, M. Broekgaarden, M. Krekorian, L.K. Alles, A.C. van Wijk, C. Mackaaij, J. Verheij, A.C. van der Wal, T.M. van Gulik, G. Storm, et al., Inhibition of hypoxia inducible factor 1 and topoisomerase with acriflavine sensitizes perihilar

- cholangiocarcinomas to photodynamic therapy, Oncotarget. 7 (3) (2016)
- [11] R. Weijer, M. Broekgaarden, R.F. van Golen, E. Bulle, E. Nieuwenhuis, A. Jongejan, P.D. Moerland, A.H. van Kampen, T.M. van Gulik, M. Heger, Low-power photodynamic therapy induces survival signaling in perihilar cholangiocarcinoma cells, BMC Cancer 15 (2015) 1014.
- [12] M. Broekgaarden, R. Weijer, A.C. van Wijk, R.C. Cox, M.R. Egmond, R. Hoebe, T. M. van Gulik, M. Heger, Photodynamic therapy with liposomal zinc phthalocyanine and tirapazamine increases tumor cell death via DNA damage, J. Biomed. Nanotechnol. 13 (2) (2017) 204–220.
- [13] J. Valle, H. Wasan, D.H. Palmer, D. Cunningham, A. Anthoney, A. Maraveyas, S. Madhusudan, T. Iveson, S. Hughes, S.P. Pereira, et al., Cisplatin plus gemcitabine versus gemcitabine for biliary tract cancer, N. Engl. J. Med. 362 (14) (2010) 1273–1281.
- [14] T. Zoepf, R. Jakobs, J.C. Arnold, D. Apel, J.F. Riemann, Palliation of nonresectable bile duct cancer: improved survival after photodynamic therapy, Am. J. Gastroenterol. 100 (11) (2005) 2426–2430.
- [15] R.V. Stan, D. Tse, S.J. Deharvengt, N.C. Smits, Y. Xu, M.R. Luciano, C.L. McGarry, M. Buitendijk, K.V. Nemani, R. Elgueta, et al., The diaphragms of fenestrated endothelia: gatekeepers of vascular permeability and blood composition, Dev. Cell 23 (6) (2012) 1203–1218.
- [16] H. Sarin, Physiologic upper limits of pore size of different blood capillary types and another perspective on the dual pore theory of microvascular permeability, J. Angiogenes. Res. 2 (2010) 14.
- [17] M. Broekgaarden, R. Weijer, M. Krekorian, B. van den Ijssel, M. Kos, L.K. Alles, A. C. van Wijk, Z. Bikadi, E. Hazai, T.M. van Gulik, et al., Inhibition of hypoxia-inducible factor 1 with acriflavine sensitizes hypoxic tumor cells to photodynamic therapy with zinc phthalocyanine-encapsulating cationic liposomes, Nano Res. 9 (6) (2016) 1639–1662.
- [18] M. Broekgaarden, R. van Vught, S. Oliveira, R.C. Roovers, P.M. Van Bergen en Henegouwen, R.J. Pieters, T.M. Van Gulik, E. Breukink, M. Heger, Site-specific conjugation of single domain antibodies to liposomes enhances photosensitizer uptake and photodynamic therapy efficacy, Nanoscale, 8 (12) (2016) 6490–6494.
- [19] G. Thurston, J.W. McLean, M. Rizen, P. Baluk, A. Haskell, T.J. Murphy, D. Hanahan, D.M. McDonald, Cationic liposomes target angiogenic endothelial cells in tumors and chronic inflammation in mice, J. Clin. Invest. 101 (7) (1998) 1401–1413.
- [20] R. Gilabert-Oriol, G.M. Ryan, A.W.Y. Leung, N.S. Firmino, K.L. Bennewith, M. B. Bally, Liposomal formulations to modulate the tumour microenvironment and antitumour immune response, Int. J. Mol. Sci. 19 (2018) 10.
- [21] M.I. van Raath, R. Weijer, G.H. Nguyen, B. Choi, A.I. de Kroon, M. Heger, Tranexamic acid-encapsulating thermosensitive liposomes for site-specific pharmaco-laser therapy of port wine stains, J. Biomed. Nanotechnol. 12 (8) (2016) 1617–1640.
- [22] W.S. Chan, J.F. Marshall, R. Svensen, J. Bedwell, I.R. Hart, Effect of sulfonation on the cell and tissue distribution of the photosensitizer aluminum phthalocyanine, Cancer Res. 50 (15) (1990) 4533–4538.
- [23] Q. Peng, J. Moan, Correlation of distribution of sulphonated aluminium phthalocyanines with their photodynamic effect in tumour and skin of mice bearing CaD2 mammary carcinoma, Br. J. Cancer 72 (3) (1995) 565–574.
- [24] M. Ochsner, Light scattering of human skin: a comparison between zinc (II)phthalocyanine and photofrin II, J. Photochem. Photobiol. B 32 (1–2) (1996) 3–9.
- [25] N. Brasseur, R. Ouellet, C. La Madeleine, J.E. van Lier, Water-soluble aluminium phthalocyanine-polymer conjugates for PDT: photodynamic activities and pharmacokinetics in tumour-bearing mice, Br. J. Cancer 80 (10) (1999) 1533–1541.
- [26] R. Weijer, S. Clavier, E.A. Zaal, M.M. Pijls, R.T. van Kooten, K. Vermaas, R. Leen, A. Jongejan, P.D. Moerland, A.H. van Kampen, et al., Multi-OMIC profiling of survival and metabolic signaling networks in cells subjected to photodynamic therapy, Cell. Mol. Life Sci. 74 (6) (2017) 1133–1151.
- [27] J.D. Spikes, Phthalocyanines as photosensitizers in biological systems and for the photodynamic therapy of tumors, Photochem. Photobiol. 43 (6) (1986) 691–699.
- [28] V.H. Fingar, T.J. Wieman, P.S. Karavolos, K.W. Doak, R. Ouellet, J.E. van Lier, The effects of photodynamic therapy using differently substituted zinc phthalocyanines on vessel constriction, vessel leakage and tumor response, Photochem. Photobiol. 58 (2) (1993) 251–258.
- [29] Y. Huang, G. Xu, Y. Peng, H. Lin, X. Zheng, M. Xie, Zinc phthalocyanine tetrasulfonate (ZnPcS4): a new photosensitizer for photodynamic therapy in choroidal neovascularization, J. Ocul. Pharmacol. Ther. 23 (4) (2007) 377–386.
- [30] C.N. Lemos, J.G. de Souza, P.S. Simao, R.F. Lopez, Iontophoresis improved growth reduction of invasive squamous cell carcinoma in topical photodynamic therapy, PLoS One 11 (1) (2016), e0145922.
- [31] A. Viola, A. Jeunet, R. Decreau, M. Chanon, M. Julliard, ESR studies of a series of phthalocyanines. Mechanism of phototoxicity. Comparative quantitation of O2-. Using ESR spin-trapping and cytochrome c reduction techniques, Free Radic. Res. 28 (5) (1998) 517–532.
- [32] E.D. Almeida, L.V. Dipieri, F.C. Rossetti, J.M. Marchetti, M. Bentley, R.S. Nunes, V.H. Sarmento, M.E.G. Valerio, J.J. Rodrigues Junior, M.M. Montalvao, et al., Skin permeation, biocompatibility and antitumor effect of chloroaluminum phthalocyanine associated to oleic acid in lipid nanoparticles, Photodiagn. Photodyn. Ther. 24 (2018) 262–273.
- [33] P.L. Goto, M.P. Siqueira-Moura, A.C. Tedesco, Application of aluminum chloride phthalocyanine-loaded solid lipid nanoparticles for photodynamic inactivation of melanoma cells, Int. J. Pharm. 518 (1–2) (2017) 228–241.
- [34] M.P. Siqueira-Moura, F.L. Primo, E.M. Espreafico, A.C. Tedesco, Development, characterization, and photocytotoxicity assessment on human melanoma of

- chloroaluminum phthalocyanine nanocapsules, Mater. Sci. Eng. C Mater. Biol. Appl. 33 (3) (2013) 1744–1752.
- [35] M.S. Rocha, C.M. Lucci, J.P. Longo, P.D. Galera, A.R. Simioni, Z.G. Lacava, A. C. Tedesco, R.B. Azevedo, Aluminum-chloride-phthalocyanine encapsulated in liposomes: activity against naturally occurring dog breast cancer cells, J. Biomed. Nanotechnol. 8 (2) (2012) 251–257.
- [36] J.P. Longo, S.C. Leal, A.R. Simioni, M. de Fatima Menezes Almeida-Santos, A. C. Tedesco, R.B. Azevedo, Photodynamic therapy disinfection of carious tissue mediated by aluminum-chloride-phthalocyanine entrapped in cationic liposomes: an in vitro and clinical study, Lasers Med. Sci. 27 (3) (2012) 575–584.
- [37] K. Komatsu, Photodynamic cell killing effects and acute skin photosensitivity of aluminum-chloro-tetrasulfonated phthalocyanine and hematoporphyrin derivative, Jpn. J. Cancer Res. 82 (5) (1991) 599–606.
- [38] Tetko IV, Virtual Computational Chemistry Laboratory, 2021. http://www.vcclab. Accessed May, 2020.
- [39] Y. Chin, S.H. Lim, Y. Zorlu, V. Ahsen, L.V. Kiew, L.Y. Chung, F. Dumoulin, H. B. Lee, Improved photodynamic efficacy of Zn(II) phthalocyanines via glycerol substitution, PLoS One 9 (5) (2014), e97894.
- [40] L. Polo, A. Segalla, G. Jori, G. Bocchiotti, G. Verna, R. Franceschini, R. Mosca, P. G. De Filippi, Liposome-delivered 131I-labelled Zn(II)-phthalocyanine as a radiodiagnostic agent for tumours, Cancer Lett. 109 (1–2) (1996) 57–61.
- [41] E. Reddi, C. Zhou, R. Biolo, E. Menegaldo, G. Jori, Liposome- or LDL-administered Zn (II)-phthalocyanine as a photodynamic agent for tumours. I. Pharmacokinetic properties and phototherapeutic efficiency, Br. J. Cancer 61 (3) (1990) 407–411.
- [42] E. Reddi, G. Lo Castro, R. Biolo, G. Jori, Pharmacokinetic studies with zinc(II)-phthalocyanine in tumour-bearing mice, Br. J. Cancer 56 (5) (1987) 597–600.
- [43] H.L. van Leengoed, N. van der Veen, A.A. Versteeg, R. Ouellet, J.E. van Lier, W. M. Star, In vivo fluorescence kinetics of phthalocyanines in a skin-fold observation chamber model: role of central metal ion and degree of sulfonation, Photochem. Photobiol. 58 (2) (1993) 233–237.
- [44] E.C. Tapajos, J.P. Longo, A.R. Simioni, Z.G. Lacava, M.F. Santos, P.C. Morais, A. C. Tedesco, R.B. Azevedo, In vitro photodynamic therapy on human oral keratinocytes using chloroaluminum-phthalocyanine, Oral Oncol. 44 (11) (2008) 1073–1079.
- [45] E. Ricci-Junior, J.M. Marchetti, Zinc(II) phthalocyanine loaded PLGA nanoparticles for photodynamic therapy use, Int. J. Pharm. 310 (1–2) (2006) 187–195.
- [46] J. Taillefer, M.C. Jones, N. Brasseur, J.E. van Lier, J.C. Leroux, Preparation and characterization of pH-responsive polymeric micelles for the delivery of photosensitizing anticancer drugs, J. Pharm. Sci. 89 (1) (2000) 52–62.
- [47] R.M. Amin, C. Hauser, I. Kinzler, A. Rueck, C. Scalfi-Happ, Evaluation of photodynamic treatment using aluminum phthalocyanine tetrasulfonate chloride as a photosensitizer: new approach, Photochem. Photobiol. Sci. 11 (7) (2012) 1156–1163.
- [48] L.A. Muehlmann, B.C. Ma, J.P. Longo, M.F. de Almeida Santos, R.B. Azevedo, Aluminum-phthalocyanine chloride associated to poly(methyl vinyl ether-comaleic anhydride) nanoparticles as a new third-generation photosensitizer for anticancer photodynamic therapy, Int. J. Nanomedicine 9 (2014) 1199–1213.
- [49] M. Zhang, R.R. Naik, L. Dai, Carbon Nanomaterials for Biomedical Applications, Cham Springer International Publishing, 2016.
- [50] L.A. Muehlmann, M.C. Rodrigues, J.P. Longo, M.P. Garcia, K.R. Py-Daniel, A. B. Veloso, P.E. de Souza, S.W. da Silva, R.B. Azevedo, Aluminium-phthalocyanine chloride nanoemulsions for anticancer photodynamic therapy: Development and in vitro activity against monolayers and spheroids of human mammary adenocarcinoma MCF-7 cells, J. Nanobiotechnol. 13 (2015) 36.
- [51] B.W. Henderson, T.J. Dougherty, Photodynamic therapy: Basic principles and clinical applications, Marcel Dekker, New York, 1992.
- [52] M.J. Bovis, J.H. Woodhams, M. Loizidou, D. Scheglmann, S.G. Bown, A. J. Macrobert, Improved in vivo delivery of m-THPC via pegylated liposomes for use in photodynamic therapy, J. Control. Release 157 (2) (2012) 196–205.
- [53] J. Buchholz, B. Kaser-Hotz, T. Khan, C. Rohrer Bley, K. Melzer, R.A. Schwendener, M. Roos, H. Walt, Optimizing photodynamic therapy: in vivo pharmacokinetics of liposomal meta-(tetrahydroxyphenyl)chlorin in feline squamous cell carcinoma, Clin. Cancer Res. 11 (20) (2005) 7538–7544.
- [54] G. Rouser, S. Fkeischer, A. Yamamoto, Two dimensional then layer chromatographic separation of polar lipids and determination of phospholipids by phosphorus analysis of spots, Lipids. 5 (5) (1970) 494–496.
- [55] M.V. Berridge, P.M. Herst, A.S. Tan, Tetrazolium dyes as tools in cell biology: new insights into their cellular reduction, Biotechnol. Annu. Rev. 11 (2005) 127–152.
- [56] F.J. Bock, S.W.G. Tait, Mitochondria as multifaceted regulators of cell death, Nat. Rev. Mol. Cell Biol. 21 (2) (2020) 85–100.
- [57] V. Vichai, K. Kirtikara, Sulforhodamine B colorimetric assay for cytotoxicity screening, Nat. Protoc. 1 (3) (2006) 1112–1116.
- [58] M. Seshadri, J.A. Spernyak, R. Mazurchuk, S.H. Camacho, A.R. Oseroff, R. T. Cheney, D.A. Bellnier, Tumor vascular response to photodynamic therapy and the antivascular agent 5,6-dimethylxanthenone-4-acetic acid: implications for combination therapy, Clin. Cancer Res. 11 (11) (2005) 4241–4250.
- [59] W. Wang, L.T. Moriyama, V.S. Bagnato, Photodynamic therapy induced vascular damage: an overview of experimental PDT, Laser Phys. Lett. 10 (2) (2012), 023001.
- [60] D. Wlodkowic, J. Skommer, Z. Darzynkiewicz, Flow cytometry-based apoptosis detection, Methods Mol. Biol. 559 (2009) 19–32.
- [61] J.V. Watson, S.H. Chambers, P.J. Smith, A pragmatic approach to the analysis of DNA histograms with a definable G1 peak, Cytometry. 8 (1) (1987) 1–8.

- [62] M. Broekgaarden, M. Kos, F.A. Jurg, A.A. van Beek, T.M. van Gulik, M. Heger, Inhibition of NF-kappaB in tumor cells exacerbates immune cell activation following photodynamic therapy, Int. J. Mol. Sci. 16 (8) (2015) 19960–19977.
- [63] M.J. Reiniers, R.F. van Golen, S. Bonnet, M. Broekgaarden, T.M. van Gulik, M. R. Egmond, M. Heger, Preparation and practical applications of 2',7'-dichlorodihydrofluorescein in redox assays, Anal. Chem. 89 (7) (2017) 3853–3857.
- [64] M. Broekgaarden, R. Weijer, T.M. van Gulik, M.R. Hamblin, M. Heger, Tumor cell survival pathways activated by photodynamic therapy: a molecular basis for pharmacological inhibition strategies, Cancer Metastasis Rev. 34 (4) (2015) 643–690.
- [65] B.A. Allison, P.H. Pritchard, J.G. Levy, Evidence for low-density lipoprotein receptor-mediated uptake of benzoporphyrin derivative, Br. J. Cancer 69 (5) (1994) 833–839.
- [66] L. Polo, G. Bianco, E. Reddi, G. Jori, The effect of different liposomal formulations on the interaction of Zn(II)-phthalocyanine with isolated low and high density lipoproteins, Int. J. Biochem. Cell Biol. 27 (12) (1995) 1249–1255.
- [67] O. Arrieta, L.A. Medina, E. Estrada-Lobato, L.A. Ramirez-Tirado, V.O. Mendoza-Garcia, J. de la Garza-Salazar, High liposomal doxorubicin tumour tissue distribution, as determined by radiopharmaceutical labelling with (99m)Tc-LD, is associated with the response and survival of patients with unresectable pleural mesothelioma treated with a combination of liposomal doxorubicin and cisplatin, Cancer Chemother. Pharmacol. 74 (1) (2014) 211–215.
- [68] D. Crivellari, K.P. Gray, S. Dellapasqua, F. Puglisi, K. Ribi, K.N. Price, I. Lang, L. Gianni, S. Spazzapan, G. Pinotti, et al., Adjuvant pegylated liposomal doxorubicin for older women with endocrine nonresponsive breast cancer who are not suitable for a "standard chemotherapy regimen": the CASA randomized trial, Breast. 22 (2) (2013) 130–137.
- [69] A.Y. Bedikian, J.A. Silverman, N.E. Papadopoulos, K.B. Kim, A.E. Hagey, A. Vardeleon, W.J. Hwu, J. Homsi, M. Davies, P. Hwu, Pharmacokinetics and safety of Marqibo (vincristine sulfate liposomes injection) in cancer patients with impaired liver function, J. Clin. Pharmacol. 51 (8) (2011) 1205–1212.
- [70] M.A. Rodriguez, R. Pytlik, T. Kozak, M. Chhanabhai, R. Gascoyne, B. Lu, S. R. Deitcher, J.N. Winter, I. Marqibo, Vincristine sulfate liposomes injection (Marqibo) in heavily pretreated patients with refractory aggressive non-Hodgkin lymphoma: report of the pivotal phase 2 study, Cancer. 115 (15) (2009) 3475–3482.
- [71] S. DiGiulio, FDA approves Onivyde combo regimen for advanced pancreatic cancer, Oncol. Times 37 (22) (2015) 8.
- [72] J. Rousseau, R. Langlois, H. Ali, J.E. van Lier, Biological activities of phthalocyanines. XII: synthesis tumor uptake and biodistribution of 14C-labeled disulfonated and trisulfonated gallium phthalocyanine in C3H mice, J. Photochem. Photobiol. B 6 (1–2) (1990) 121–132.
- [73] C.J. Tralau, H. Barr, D.R. Sandeman, T. Barton, M.R. Lewin, S.G. Bown, Aluminum sulfonated phthalocyanine distribution in rodent tumors of the colon, brain and pancreas, Photochem. Photobiol. 46 (5) (1987) 777–781.
- [74] D. Kessel, N.L. Oleinick, Cell death pathways associated with photodynamic therapy: an update, Photochem. Photobiol. 94 (2) (2018) 213–218.
- [75] C. Donohoe, M.O. Senge, L.G. Arnaut, L.C. Gomes-da-Silva, Cell death in photodynamic therapy: from oxidative stress to anti-tumor immunity, Biochim. Biophys. Acta Rev. Cancer 1872 (2) (2019) 188308.
- [76] W.K. Martins, N.F. Santos, C.S. Rocha, I.O. Bacellar, T.M. Tsubone, A.C. Viotto, A. Y. Matsukuma, A.B. Abrantes, P. Siani, L.G. Dias, et al., Parallel damage in mitochondria and lysosomes is an efficient way to photoinduce cell death, Autophagy. 15 (2) (2019) 259–279.
- [77] D.W. Edwardson, A.M. Parissenti, A.T. Kovala, Chemotherapy and inflammatory cytokine signalling in cancer cells and the tumour microenvironment, Adv. Exp. Med. Biol. 1152 (2019) 173–215.
- [78] S.V. Singh, A.K. Ajay, N. Mohammad, P. Malvi, B. Chaube, A.S. Meena, M.K. Bhat, Proteasomal inhibition sensitizes cervical cancer cells to mitomycin C-induced bystander effect: the role of tumor microenvironment, Cell Death Dis. 6 (2015) e1934.
- [79] J.V. McCann, J.L. Null, A.C. Dudley, Deadly DAaRTS destroy cancer cells via a tumor microenvironment-mediated trigger, J. Clin. Invest. 128 (7) (2018) 2750–2753
- [80] B.W. Henderson, S.M. Waldow, T.S. Mang, W.R. Potter, P.B. Malone, T. J. Dougherty, Tumor destruction and kinetics of tumor cell death in two experimental mouse tumors following photodynamic therapy, Cancer Res. 45 (2) (1985) 572–576.
- [81] V.H. Fingar, T.J. Wieman, K.W. Doak, Role of thromboxane and prostacyclin release on photodynamic therapy-induced tumor destruction, Cancer Res. 50 (9) (1990) 2599–2603.
- [82] B.W. Henderson, B. Owczarczak, J. Sweeney, T. Gessner, Effects of photodynamic treatment of platelets or endothelial cells in vitro on platelet aggregation, Photochem. Photobiol. 56 (4) (1992) 513–521.
- [83] M.W. Reed, F.N. Miller, T.J. Wieman, M.T. Tseng, C.G. Pietsch, The effect of photodynamic therapy on the microcirculation, J. Surg. Res. 45 (5) (1988) 452–459.
- [84] M. Heger, I.I. Salles, W. van Vuure, I.H. Hamelers, A.I. de Kroon, H. Deckmyn, J. F. Beek, On the interaction of fluorophore-encapsulating PEGylated lecithin liposomes with hamster and human platelets, Microvasc. Res. 78 (1) (2009) 57–66.
- [85] M. Reiss, D.E. Brash, T. Munoz-Antonia, J.A. Simon, A. Ziegler, V.F. Vellucci, Z. L. Zhou, Status of the p53 tumor suppressor gene in human squamous carcinoma cell lines, Oncol. Res. 4 (8–9) (1992) 349–357.
- [86] W.G. Kaelin Jr., The p53 gene family, Oncogene. 18 (53) (1999) 7701-7705.

- [87] L.F. Gulli, K.C. Palmer, Y.Q. Chen, K.B. Reddy, Epidermal growth factor-induced apoptosis in A431 cells can be reversed by reducing the tyrosine kinase activity, Cell Growth Differ. 7 (2) (1996) 173–178.
- [88] N. Normanno, A. De Luca, C. Bianco, L. Strizzi, M. Mancino, M.R. Maiello, A. Carotenuto, G. De Feo, F. Caponigro, D.S. Salomon, Epidermal growth factor receptor (EGFR) signaling in cancer, Gene. 366 (1) (2006) 2–16.
- [89] T. Tsai, H.T. Ji, P.C. Chiang, R.H. Chou, W.S. Chang, C.T. Chen, ALA-PDT results in phenotypic changes and decreased cellular invasion in surviving cancer cells, Lasers Surg. Med. 41 (4) (2009) 305–315.
- [90] C. Fabris, G. Valduga, G. Miotto, L. Borsetto, G. Jori, S. Garbisa, E. Reddi, Photosensitization with zinc (II) phthalocyanine as a switch in the decision between apoptosis and necrosis, Cancer Res. 61 (20) (2001) 7495–7500.
- [91] E. Ben-Hur, M. Green, A. Prager, R. Kol, I. Rosenthal, Phthalocyanine photosensitization of mammalian cells: biochemical and ultrastructural effects, Photochem. Photobiol. 46 (5) (1987) 651–656.
- [92] M.M. Qualls, D.H. Thompson, Chloroaluminum phthalocyanine tetrasulfonate delivered via acid-labile diplasmenylcholine-folate liposomes: intracellular localization and synergistic phototoxicity, Int. J. Cancer 93 (3) (2001) 384–392.
- [93] M. Idowu, T. Nyokong, Photophysical and photochemical properties of zinc and aluminum phthalocyanines in the presence of magnetic fluid, J. Photochem. Photobiol. A. 188 (2) (2007) 200–206.
- [94] J.W. Owens, R. Smith, R. Robinson, M. Robins, Photophysical properties of porphyrins, phthalocyanines, and benzochlorins, Inorg. Chim. Acta 279 (2) (1998) 226–231.
- [95] N. Dan, Effect of liposome charge and PEG polymer layer thickness on cell-liposome electrostatic interactions, Biochim. Biophys. Acta 1564 (2) (2002) 343–348.
- [96] C. Corbo, R. Molinaro, F. Taraballi, N.E. Toledano Furman, M.B. Sherman, A. Parodi, F. Salvatore, E. Tasciotti, Effects of the protein corona on liposomeliposome and liposome-cell interactions, Int. J. Nanomedicine 11 (2016) 3049–3063.
- [97] J.B. Allison, R.S. Becker, Effect of metal atom perturbations on the luminescent spectra of porphyrins, J. Chem. Phys. 32 (5) (1960) 1410–1417.
- [98] P.G. Seybold, M. Gouterman, Porphyrins: XIII: fluorescence spectra and quantum yields, J. Mol. Spectrosc. 31 (1) (1969) 1–13.
- [99] I. McCubbin, D. Phillips, The photophysics and photostability of zinc(II) and aluminium(III) sulphonated naphthalocyanines, J. Photochem. 34 (2) (1986) 187-195
- [100] K.W. Woodburn, N.J. Vardaxis, J.S. Hill, A.H. Kaye, D.R. Phillips, Subcellular localization of porphyrins using confocal laser scanning microscopy, Photochem. Photobiol. 54 (5) (1991) 725–732.
- [101] J. Soriano, A. Villanueva, J.C. Stockert, M. Canete, Vehiculization determines the endocytic internalization mechanism of Zn(II)-phthalocyanine, Histochem. Cell Biol. 139 (1) (2013) 149–160.
- [102] B. Paquette, H. Ali, R. Langlois, J.E. van Lier, Biological activities of phthalocyanines-VIII. Cellular distribution in V-79 Chinese hamster cells and phototoxicity of selectively sulfonated aluminum phthalocyanines, Photochem. Photobiol. 47 (2) (1988) 215–220.
- [103] T.M. Tsubone, W.K. Martins, C. Pavani, H.C. Junqueira, R. Itri, M.S. Baptista, Enhanced efficiency of cell death by lysosome-specific photodamage, Sci. Rep. 7 (1) (2017) 6734.
- [104] B.C. Wilson, M. Olivo, G. Singh, Subcellular localization of Photofrin and aminolevulinic acid and photodynamic cross-resistance in vitro in radiationinduced fibrosarcoma cells sensitive or resistant to photofrin-mediated photodynamic therapy, Photochem. Photobiol. 65 (1) (1997) 166–176.
- [105] Z. Ji, G. Yang, V. Vasovic, B. Cunderlikova, Z. Suo, J.M. Nesland, Q. Peng, Subcellular localization pattern of protoporphyrin IX is an important determinant for its photodynamic efficiency of human carcinoma and normal cell lines, J. Photochem. Photobiol. B 84 (3) (2006) 213–220.
- [106] M.H. Teiten, L. Bezdetnaya, P. Morliere, R. Santus, F. Guillemin, Endoplasmic reticulum and Golgi apparatus are the preferential sites of Foscan localisation in cultured tumour cells, Br. J. Cancer 88 (1) (2003) 146–152.
- [107] Y.J. Hsieh, C.C. Wu, C.J. Chang, J.S. Yu, Subcellular localization of Photofrin determines the death phenotype of human epidermoid carcinoma A431 cells triggered by photodynamic therapy: when plasma membranes are the main targets, J. Cell. Physiol. 194 (3) (2003) 363–375.
- [108] M.V. Jain, A.M. Paczulla, T. Klonisch, F.N. Dimgba, S.B. Rao, K. Roberg, F. Schweizer, C. Lengerke, P. Davoodpour, V.R. Palicharla, et al., Interconnections between apoptotic, autophagic and necrotic pathways: implications for cancer therapy development, J. Cell. Mol. Med. 17 (1) (2013) 12–29.
- [109] K.M. Kadish, K.M. Smith, R. Guilard, The porphyrin handbook Vol. 17: Phthalocyanines: Properties and materials, Academic Press, San Diego, 2003.
- [110] H.B. Ris, H.J. Altermatt, B. Nachbur, J.C. Stewart, Q. Wang, C.K. Lim, R. Bonnett, U. Althaus, Effect of drug-light interval on photodynamic therapy with metatetrahydroxyphenylchlorin in malignant mesothelioma, Int. J. Cancer 53 (1) (1993) 141–146.
- [111] B.W. Henderson, V.H. Fingar, Relationship of tumor hypoxia and response to photodynamic treatment in an experimental mouse tumor, Cancer Res. 47 (12) (1987) 3110–3114.
- [112] B.D. Hirsch, N.C. Walz, B.E. Meeker, M.R. Arnfield, J. Tulip, M.S. McPhee, J. D. Chapman, Photodynamic therapy-induced hypoxia in rat tumors and normal tissues, Photochem. Photobiol. 46 (5) (1987) 847–852.
- [113] J.D. Chapman, M.S. McPhee, N. Walz, M.P. Chetner, C.C. Stobbe, K. Soderlind, M. Arnfield, B.E. Meeker, L. Trimble, P.S. Allen, Nuclear magnetic resonance spectroscopy and sensitizer-adduct measurements of photodynamic therapy-induced ischemia in solid tumors, J. Natl. Cancer Inst. 83 (22) (1991) 1650–1659.

- [114] D. Kessel, Y. Luo, Mitochondrial photodamage and PDT-induced apoptosis, J. Photochem. Photobiol. B 42 (2) (1998) 89–95.
- [115] D.E. Dolmans, A. Kadambi, J.S. Hill, C.A. Waters, B.C. Robinson, J.P. Walker, D. Fukumura, R.K. Jain, Vascular accumulation of a novel photosensitizer, MV6401, causes selective thrombosis in tumor vessels after photodynamic therapy, Cancer Res. 62 (7) (2002) 2151–2156.
- [116] C. Hadjur, G. Wagnieres, F. Ihringer, P. Monnier, H. van den Bergh, Production of the free radicals O2.- and .OH by irradiation of the photosensitizer zinc(II) phthalocyanine, J. Photochem. Photobiol. B 38 (2–3) (1997) 196–202.
- [117] I. Rosenthal, C. Murali Krishna, P. Riesz, E. Ben-Hur, The role of molecular oxygen in the photodynamic effect of phthalocyanines, Radiat. Res. 107 (1) (1986) 136–142.
- [118] G. Valduga, S. Nonell, E. Reddi, G. Jori, S.E. Braslavsky, The production of singlet molecular oxygen by zinc(II) phthalocyanine in ethanol and in unilamellar vesicles. Chemical quenching and phosphorescence studies, Photochem. Photobiol. 48 (1) (1988) 1–5.
- [119] P.R. Ogilby, Singlet oxygen: there is indeed something new under the sun, Chem. Soc. Rev. 39 (8) (2010) 3181–3209.
- [120] S.W. Ryter, R.M. Tyrrell, Singlet molecular oxygen ((1)02): a possible effector of eukaryotic gene expression, Free Radic. Biol. Med. 24 (9) (1998) 1520–1534.
- [121] M.J. Davies, Reactive species formed on proteins exposed to singlet oxygen, Photochem. Photobiol. Sci. 3 (1) (2004) 17–25.
- [122] F.C. Cheng, J.F. Jen, T.H. Tsai, Hydroxyl radical in living systems and its separation methods, J. Chromatogr. B Anal. Technol. Biomed. Life Sci. 781 (1–2) (2002) 481–496.
- [123] Y. Sueishi, M. Hori, M. Ishikawa, K. Matsu-Ura, E. Kamogawa, Y. Honda, M. Kita, K. Ohara, Scavenging rate constants of hydrophilic antioxidants against multiple reactive oxygen species, J. Clin. Biochem. Nutr. 54 (2) (2014) 67–74.
- [124] R.F. van Golen, T.M. van Gulik, M. Heger, Mechanistic overview of reactive species-induced degradation of the endothelial glycocalyx during hepatic ischemia/reperfusion injury, Free Radic. Biol. Med. 52 (8) (2012) 1382–1402.
- [125] S. Mitroka, S. Zimmeck, D. Troya, J.M. Tanko, How solvent modulates hydroxyl radical reactivity in hydrogen atom abstractions, J. Am. Chem. Soc. 132 (9) (2010) 2907–2913.
- [126] Y. Yuan, C.J. Zhang, S. Xu, B. Liu, A self-reporting AIE probe with a built-in singlet oxygen sensor for targeted photodynamic ablation of cancer cells, Chem. Sci. 7 (3) (2016) 1862–1866.
- [127] A. Reis, C.M. Spickett, Chemistry of phospholipid oxidation, Biochim. Biophys. Acta 1818 (10) (2012) 2374–2387.
- [128] H. Yin, L. Xu, N.A. Porter, Free radical lipid peroxidation: mechanisms and analysis, Chem. Rev. 111 (10) (2011) 5944–5972.
- [129] M.M. Gaschler, B.R. Stockwell, Lipid peroxidation in cell death, Biochem. Biophys. Res. Commun. 482 (3) (2017) 419–425.
- [130] W.Y. Tai, Y.C. Yang, H.J. Lin, C.P. Huang, Y.L. Cheng, M.F. Chen, H.L. Yen, I. Liau, Interplay between structure and fluidity of model lipid membranes under oxidative attack, J. Phys. Chem. B 114 (47) (2010) 15642–15649.
- [131] A. Vantieghem, Y. Xu, W. Declercq, P. Vandenabeele, G. Denecker, J. R. Vandenheede, W. Merlevede, P.A. de Witte, P. Agostinis, Different pathways mediate cytochrome c release after photodynamic therapy with hypericin, Photochem. Photobiol. 74 (2) (2001) 133–142.
- [132] J.J. Lemasters, A.L. Nieminen, T. Qian, L.C. Trost, S.P. Elmore, Y. Nishimura, R. A. Crowe, W.E. Cascio, C.A. Bradham, D.A. Brenner, et al., The mitochondrial permeability transition in cell death: a common mechanism in necrosis, apoptosis and autophagy, Biochim. Biophys. Acta 1366 (1–2) (1998) 177–196.
- [133] P. Mroz, A. Yaroslavsky, G.B. Kharkwal, M.R. Hamblin, Cell death pathways in photodynamic therapy of cancer, Cancers (Basel) 3 (2) (2011) 2516–2539.
- [134] P.A. Tsaytler, M. Cof, D.V. Sakharov, J. Krijgsveld, M.R. Egmond, Immediate protein targets of photodynamic treatment in carcinoma cells, J. Proteome Res. 7 (9) (2008) 3868–3878.
- [135] J. Morgan, A.R. Oseroff, Mitochondria-based photodynamic anti-cancer therapy, Adv. Drug Deliv. Rev. 49 (1–2) (2001) 71–86.
- [136] S. Aits, M. Jaattela, Lysosomal cell death at a glance, J. Cell Sci. 126 (Pt 9) (2013) 1905–1912
- [137] I. Beltran Hernandez, Y. Yu, F. Ossendorp, M. Korbelik, S. Oliveira, Preclinical and clinical evidence of immune responses triggered in oncologic photodynamic therapy: clinical recommendations, J. Clin. Med. 9 (2020) 2.
- [138] G. Sun, D.J. Montell, Q&A: cellular near death experiences-what is anastasis? BMC Biol. 15 (1) (2017) 92.
- [139] J. Bazak, J.M. Fahey, K. Wawak, W. Korytowski, A.W. Girotti, Enhanced aggressiveness of bystander cells in an anti-tumor photodynamic therapy model: Role of nitric oxide produced by targeted cells, Free Radic. Biol. Med. 102 (2017) 111–121.
- [140] N. Solban, P.K. Selbo, A.K. Sinha, S.K. Chang, T. Hasan, Mechanistic investigation and implications of photodynamic therapy induction of vascular endothelial growth factor in prostate cancer, Cancer Res. 66 (11) (2006) 5633–5640.
- [141] C.S. Shim, Y.K. Cheon, S.W. Cha, S. Bhandari, J.H. Moon, Y.D. Cho, Y.S. Kim, L. S. Lee, M.S. Lee, B.S. Kim, Prospective study of the effectiveness of percutaneous

- transhepatic photodynamic therapy for advanced bile duct cancer and the role of intraductal ultrasonography in response assessment, Endoscopy. 37 (5) (2005) 425–433
- [142] S.A. Thompson, A. Aggarwal, S. Singh, A.P. Adam, J.P.C. Tome, C.M. Drain, Compromising the plasma membrane as a secondary target in photodynamic therapy-induced necrosis, Bioorg. Med. Chem. 26 (18) (2018) 5224–5228.
- [143] Y. Zhang, Y.K. Cheung, D.K.P. Ng, W.P. Fong, Immunogenic necroptosis in the anti-tumor photodynamic action of BAM-SiPc, a silicon(IV) phthalocyanine-based photosensitizer, Cancer Immunol. Immunother. (2020).
- [144] M.A. Miller, J.F. Zachary, Mechanisms and morphology of cellular injury, adaptation, and death, Pathol. Basis Vet. Dis. (2017) 2–43, e19.
- [145] I.K. Poon, M.D. Hulett, C.R. Parish, Molecular mechanisms of late apoptotic/ necrotic cell clearance, Cell Death Differ. 17 (3) (2010) 381–397.
- [146] T. Vanden Berghe, N. Vanlangenakker, E. Parthoens, W. Deckers, M. Devos, N. Festjens, C.J. Guerin, U.T. Brunk, W. Declercq, P. Vandenabeele, Necroptosis, necrosis and secondary necrosis converge on similar cellular disintegration features, Cell Death Differ. 17 (6) (2010) 922–930.
- [147] S.L. Haywood-Small, D.I. Vernon, J. Griffiths, J. Schofield, S.B. Brown, Phthalocyanine-mediated photodynamic therapy induces cell death and a G0/G1 cell cycle arrest in cervical cancer cells, Biochem. Biophys. Res. Commun. 339 (2) (2006) 569–576.
- [148] Y. Tsujimoto, Apoptosis and necrosis: intracellular ATP level as a determinant for cell death modes, Cell Death Differ. 4 (6) (1997) 429–434.
- [149] I.M. Ndhundhuma, H. Abrahamse, Susceptibility of in vitro melanoma skin cancer to photoactivated hypericin versus aluminium(III) phthalocyanine chloride tetrasulphonate, Biomed. Res. Int. 2017 (2017) 5407012.
- [150] H.L. Tang, H.M. Tang, K.H. Mak, S. Hu, S.S. Wang, K.M. Wong, C.S. Wong, H. Y. Wu, H.T. Law, K. Liu, et al., Cell survival, DNA damage, and oncogenic transformation after a transient and reversible apoptotic response, Mol. Biol. Cell 23 (12) (2012) 2240–2252.
- [151] H.M. Tang, H.L. Tang, Cell recovery by reversal of ferroptosis, Biol. Open 8 (2019) 6.
- [152] Y.N. Gong, C. Guy, H. Olauson, J.U. Becker, M. Yang, P. Fitzgerald, A. Linkermann, D.R. Green, ESCRT-III acts downstream of MLKL to regulate Necroptotic cell death and its consequences, Cell. 169 (2) (2017) 286–300, e16.
- [153] M. Overholtzer, J.S. Brugge, The cell biology of cell-in-cell structures, Nat. Rev. Mol. Cell Biol. 9 (10) (2008) 796–809.
- [154] M.R. Hamblin, H. Abrahamse, Factors affecting photodynamic therapy and antitumor immune response, Anti Cancer Agents Med. Chem. 21 (2020), 123, https:// doi.org/10.2174/1871520620666200318101037.
- [155] O. Kepp, A. Marabelle, L. Zitvogel, G. Kroemer, Oncolysis without viruses inducing systemic anticancer immune responses with local therapies, Nat. Rev. Clin. Oncol. 17 (1) (2020) 49–64.
- [156] H.S. Hwang, H. Shin, J. Han, K. Na, Combination of photodynamic therapy (PDT) and anti-tumor immunity in cancer therapy, J. Pharm. Investig. 48 (2) (2018) 143–151.
- [157] J. Zhou, G. Wang, Y. Chen, H. Wang, Y. Hua, Z. Cai, Immunogenic cell death in cancer therapy: present and emerging inducers, J. Cell. Mol. Med. 23 (8) (2019) 4854–4865.
- [158] M. Sachet, Y.Y. Liang, R. Oehler, The immune response to secondary necrotic cells, Apoptosis. 22 (10) (2017) 1189–1204.
- [159] J. Gamrekelashvili, T.F. Greten, F. Korangy, Immunogenicity of necrotic cell death, Cell. Mol. Life Sci. 72 (2) (2015) 273–283.
- [160] Y.K. Dhuriya, D. Sharma, Necroptosis: a regulated inflammatory mode of cell death, J. Neuroinflammation 15 (1) (2018) 199.
- [161] N. Hoa, M.P. Myers, T.G. Douglass, J.G. Zhang, C. Delgado, L. Driggers, L. L. Callahan, G. VanDeusen, J.T. Pham, N. Bhakta, et al., Molecular mechanisms of paraptosis induction: implications for a non-genetically modified tumor vaccine, PLoS One 4 (2) (2009), e4631.
- [162] O. Krysko, T.L. Aaes, V.E. Kagan, K. D'Herde, C. Bachert, L. Leybaert, P. Vandenabeele, D.V. Krysko, Necroptotic cell death in anti-cancer therapy, Immunol. Rev. 280 (1) (2017) 207–219.
- [163] P. Vandenabeele, K. Vandecasteele, C. Bachert, O. Krysko, D.V. Krysko, Immunogenic apoptotic cell death and anticancer immunity, Adv. Exp. Med. Biol. 930 (2016) 133–149.
- [164] B. Pucci, M. Kasten, A. Giordano, Cell cycle and apoptosis, Neoplasia. 2 (4) (2000) 291–299.
- [165] P.A. Muller, K.H. Vousden, Mutant p53 in cancer: new functions and therapeutic opportunities, Cancer Cell 25 (3) (2014) 304–317.
- [166] T.J. Langan, K.R. Rodgers, R.C. Chou, Synchronization of mammalian cell cultures by serum deprivation, Methods Mol. Biol. 1524 (2017) 97–105.
- [167] A.M. Narasimha, M. Kaulich, G.S. Shapiro, Y.J. Choi, P. Sicinski, S.F. Dowdy, Cyclin D activates the Rb tumor suppressor by mono-phosphorylation, Elife (2014) 3.
- [168] N. Ahmad, D.K. Feyes, R. Agarwal, H. Mukhtar, Photodynamic therapy results in induction of WAF1/CIP1/P21 leading to cell cycle arrest and apoptosis, Proc. Natl. Acad. Sci. U. S. A. 95 (12) (1998) 6977–6982.